TECHNICAL REPORT

ISO/TR 20891

First edition
2020-10

Space systems — Space batteries — Guidelines for in-flight health assessment of lithium-ion batteries

Systèmes spatiaux - Batteries spatiales - lignes directrices pour l'évaluation en vol de la santé des batteries lithium-ion

Reference number
ISO/TR 20891:2020(E)

ISO copyright office
CP 401 • Ch. de Blandonnet 8
CH-1214 Vernier, Geneva
Phone: +41 22 749 01 11
Email: copyright@iso.org
Website: www.iso.org

Published in Switzerland

Contents

Page

Foreword

ISO (the International Organization for Standardization) is a worldwide federation of national standards bodies (ISO member bodies). The work of preparing International Standards is normally carried out through ISO technical committees. Each member body interested in a subject for which a technical committee has been established has the right to be represented on that committee. International organizations, governmental and non-governmental, in liaison with ISO, also take part in the work. ISO collaborates closely with the International Electrotechnical Commission (IEC) on all matters of electrotechnical standardization.

The procedures used to develop this document and those intended for its further maintenance are described in the ISO/IEC Directives, Part 1. In particular, the different approval criteria needed for the different types of ISO documents should be noted. This document was drafted in accordance with the editorial rules of the ISO/IEC Directives, Part 2 (see www.iso.org/directives).

Attention is drawn to the possibility that some of the elements of this document may be the subject of patent rights. ISO shall not be held responsible for identifying any or all such patent rights. Details of any patent rights identified during the development of the document will be in the Introduction and/or on the ISO list of patent declarations received (see www.iso.org/patents).

Any trade name used in this document is information given for the convenience of users and does not constitute an endorsement.

For an explanation of the voluntary nature of standards, the meaning of ISO specific terms and expressions related to conformity assessment, as well as information about ISO's adherence to the World Trade Organization (WTO) principles in the Technical Barriers to Trade (TBT), see www.iso.org/iso/foreword.html.

This document was prepared by Technical Committee ISO/TC 20, *Aircraft and space vehicles*, Subcommittee SC 14, *Space systems and operations*.

Any feedback or questions on this document should be directed to the user's national standards body. A complete listing of these bodies can be found at www.iso.org/members.html.

Introduction

The charge and discharge cycle of a battery is not 100 % efficient, with each cycle side reactions can occur that eventually accumulate and cause degradation of the battery's performance. Understanding how the battery's performance changes throughout the mission is a subject of importance; and accurate determination of the battery's current SoH is essential in a large number of situations, for example:

— the routine assessment of battery performance to allow early detection of anomalies (by comparing its actual versus predicted performance);

— the setting of alarm thresholds to ensure adequate energy;

— detection of battery anomalies that can put at risk the spacecraft passivation and/or de-orbiting strategy;

— decisions regarding mission extension beyond initial target life;

— evaluating the remaining capability of a spacecraft upon occurrence of an anomaly;

— feedback to the battery manufacturer to improve the performance predictions.

However, it is often difficult to properly assess the in-flight status, due to various factors:

— Flight electrical load profiles differ significantly to load profiles used to characterize battery performance models and the battery's SoH; for example, the total available battery capacity, which is the most important parameter, is not directly accessible during flight since its simple measurement by full discharge of the battery goes against the spacecraft operational safety.

— The quality of the accessible data from telemetry is sometimes poor: insufficient telemetry resolution and/or accuracy, lack of synchronization between related parameters like current and voltage, possibly large load consumption fluctuations introducing a high level of noise, delivery of data under a form not easy to process, etc.

— The battery is operating in flight in a way that is generally very different from the test conditions at qualification or acceptance. As a consequence, if no in-flight assessment has been made at the beginning of life, the direct comparison between current in-flight status and available ground testing data can be difficult and in any case more difficult than a comparison with the initial in-flight behaviour.

— The battery is operated under time variant conditions in a large bandwidth of different time scales, e.g. switching heater circuits vs. variations of the charge profile and eclipse length for a LEO satellite with drifting orbit. Low frequency variations introduced by drifting orbits or seasons are considered for the computation of trends and averaging over several orbits.

— The processing of data to derive the health status is not straightforward and is usually performed by identifying the ageing parameters of a model. Therefore, the representativeness of this model is a key issue. In addition, even with a good model, the results are not always satisfactory.

Therefore, it has been found of interest to provide detailed information about the means currently used or envisioned to perform in-flight battery health assessment and to make recommendations to spacecraft builders, operation managers and batteries manufacturers that would make it easier. This is the subject of this document.

It is important to highlight that, according to the definition given in 3.1.1, assessing the health status allows to verify that the battery behaves as well as or possibly better than anticipated. It is not aimed at providing an evaluation of any sort of "absolute ageing" nor to predict further evolution, even if this can be the case with some methods and their on-board implementation.

Space systems — Space batteries — Guidelines for in-flight health assessment of lithium-ion batteries

IMPORTANT — The electronic file of this document contains colours which are considered to be useful for the correct understanding of the document. Users should therefore consider printing this document using a colour printer.

1 Scope

This document provides detailed information on the various methods of assessing the health status of lithium-ion space batteries in flight and makes recommendations to battery suppliers, spacecraft manufacturers and operators to ease this assessment.

2 Normative references

The following documents are referred to in the text in such a way that some or all of their content constitutes requirements of this document. For dated references, only the edition cited applies. For undated references, the latest edition of the referenced document (including any amendments) applies.

ISO 17546, *Space systems — Lithium ion battery for space vehicles — Design and verification requirements*

3 Terms, definitions and abbreviated terms

3.1 Term and definitions

For the purposes of this document, the terms and definitions given in ISO 17546 and the following apply.

ISO and IEC maintain terminological databases for use in standardization at the following addresses:

— ISO Online browsing platform: available at https://www.iso.org/obp

— IEC Electropedia: available at http://www.electropedia.org/

3.1.1
battery health
state of the battery, which is healthy if both the amount and the rate of degradation of its performance are lower than or equal to the predicted ones at the same time into the mission

3.2 Abbreviated terms

ADC analogue to digital converter

BoL beginning of life

CC constant current

CV constant voltage

DoD depth of discharge

EIS electrochemical impedance spectroscopy

EMF electro-motive force (a.k.a. open circuit voltage)

EoC	end of charge
EoCV	end of charge voltage
EoD	end of discharge
EoDV	end of discharge voltage
EoL	end of life
ESA	European Space Agency
GEO	geostationary earth orbit
LEO	low earth orbit
NCA	nickel cobalt aluminium (lithium-ion cathode composition)
NIBHM	non-Intrusive battery health monitoring
SoC	state of charge
SoH	state of health
RTL	round trip loss

4 Overview

4.1 General

The SoH of a battery reflects its capability to fulfil the needs of a mission, i.e. whether the performance is at or above the expected level. Typically, the performance itself covers requirements such as;

a) the capability to deliver and absorb a certain amount of energy, under a certain load profile and with a defined voltage range;

b) the capability to deliver a certain power for a given duration, while maintaining a certain voltage.

Theoretically, assessing this SoH can be conceived as the simply monitoring the battery behaviour (e.g. the battery voltage) in the orbit and comparing it against previously set baselines but, in reality, it is far less straightforward.

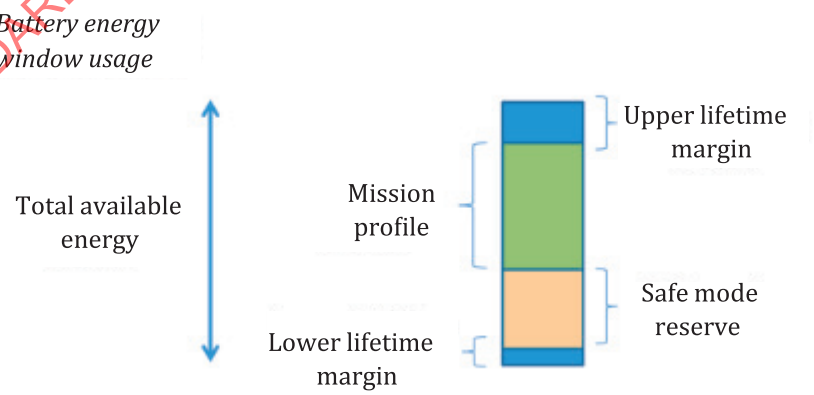

Figure 1 — Schematic of energy usage in satellite battery

As Figure 1 shows, the deliverable energy a) of a battery is dependent on the mission phase and operational strategy. In many cases this not only shows characterizing the mission energy profile but also includes understanding the proportion of contingency energy, i.e. the energy needed to reach a safe mode, as part of the recovery of a major on-board failure. There is also some usable energy that will not be used at the extremes of SoC (to mitigate the accelerated lifetime degradation that occurs with repeated use of energy in these segment of the SoC window). As energy is not expected to be drawn from the contingency or protective margins of the battery in nominal operating conditions, observing energy in these segments is simply not possible during mission.

Pulsed power profiles in b) may occur for a duration too short to be captured by the telemetry. It is thus necessary to infer the health status from only the observable data, by estimating the value of the parameters driving the battery performance.

At a simplistic level, the capabilities of the battery can be expressed using the following fundamental formulae:

$$E = QV_{\mathrm{N}} \tag{1}$$

where

E is the battery energy (Wh);

Q is the battery capacity (Ah);

V_{N} is the nominal voltage at which the charge is delivered (V).

$$V_{\mathrm{T}} = V_{\mathrm{OCV}} \pm IR \tag{2}$$

where

V_{T} is the terminal voltage (V);

V_{OCV} is the open circuit voltage of the battery (V);

I is the current in (or out) of the battery (A);

R is the resistance (or internal impedance) of the battery (Ω).

$$P = IV_{\mathrm{OCV}} \pm I^2R \tag{3}$$

Where P is the power developed by the battery (W).

$$R = R_{\Omega} + R_{\mathrm{CT}} + R_{\mathrm{dif}} \tag{4}$$

where

R_{Ω} is the ohmic (electronic) resistance (Ω);

R_{CT} is the charge transfer resistance (Ω);

R_{dif} is the diffusion resistance (Ω).

From the formulae, it can be seen that the battery capacity and voltage (driving factor of a) above) and internal impedance (driving factor of b)) are the main contributors to the battery performance and

that the evolution of these factors through ageing leads to a reduction of both the operating voltage at a given discharged energy and the discharge rate[7].

Other parameters, like self-discharge or diffusion time constant, are also quite sensitive to ageing but have, at most, a second order influence on the performance. This does not mean, though, that they cannot be useful indicators of the battery SoH.

It is worth noting that many parameters (such as resistance and SoC) have a temperature dependency, which should be considered when choosing a test temperature or interpreting telemetry data.

4.2 Battery capacity

The simplest and most direct way of measuring a battery capacity is to perform a full discharge at a known rate (the lower the current the less resistive effects that will be observed). Unfortunately, this is usually not compatible with safe operation of the spacecraft. Therefore, the difficulty of estimating the capacity depends on the way the battery is used on board.

On a GEO, the total number of eclipses over the lifetime is small and consequently the battery can be used at a relatively large DoD, in the range of 70 % to 80 %. In such operating conditions, most of the discharge curve is accessible directly via the telemetry and, given the large fraction of the orbit period that is devoted to charging, the battery has time to reach a stable state, usually taper under almost zero current.

Conversely, in a LEO, the very large number of eclipses forces to limit the operating DoD to values around 20 % and the quick succession of eclipse and sunlight regimes does not allow the battery to reach any steady state (here the diffusion plays a significant role). Furthermore, due to seasonal variations of the sun illumination and even more pronounced variations in the case of a drifting orbit, the repetitive profile of the battery state from orbit to orbit is not even converging towards a stationary profile. It is therefore much more difficult to observe directly a stable battery behaviour.

4.3 Battery impedance

4.3.1 General

A rechargeable intercalation battery functions by internal ion flow motivating external electron flow (discharge) or external electron flow motivating internal ionic movement (charge). When subjecting a cell to a flow of current, a chemical change occurs within it. This chemical change causes the build-up or dissipation of obstacles to the current. These obstacles are known as polarizations:

a) Ohmic polarization is caused by ohmic internal resistance of the cell against the flow of the current. This ohmic resistance (R_Ω) consists of an electronic resistance and an ionic one.

   — The electronic resistance can be seen in positive current collectors (foil and electrode terminal), positive active materials, positive conductive materials, negative current collectors (foil and electrode terminal) and negative active materials. Contact resistance between positive current collector and positive active materials is also an electronic resistance because the oxide thin layer is formed on the surface of the aluminium current collector foil. Since the positive active material shows a characteristic in electronic conductivity similar to a semiconductor, mixed conductive material like carbon keep electronic network in positive electrode layer. On the other hand, negative current collectors made of copper and negative active materials made of carbon have lower electronic resistance than positive ones.

   — The ionic resistance is another component of ohmic polarization. The resistance makes obstacle against the transfer of Li-ion and counter anion in liquid electrolyte impregnated in consecutive micro-pores inside the positive electrode layer, negative electrode layer and porous separator.

   This polarization usually has a very fast response time, i.e. in the order of milliseconds.

b) Activation polarization is the potential difference needed to generate currents depending on the activation energy of electrode reaction. The activation energy has electrons transferred from

electrodes into electrolyte or from electrolyte into electrodes. In the case of charge reaction of positive electrode, for example, Li de-intercalated from solid active material inside is activated on the surface of particle, and thereafter is oxidized to Li-ion. The response can be in the order of 10 milliseconds to seconds.

c) Concentration polarization denotes the voltage loss resulting from changes in the electrolyte concentration due to a flow of electrode reaction current through the electrode/electrolyte interface. The concentration polarization is equivalent to a difference of the thermodynamic potential, which is a function of concentration of electrode reaction species.

d) Diffusion polarization is a kind of concentration polarization. The diffusion polarization occurs when electrode reaction species become insufficient at the electrode surface because of slow supply rate driven by concentration gradient. This polarization occurs at the positive and negative electrode surface, for example, when Li transfer from active material to electrode surface through solid phase by diffusion process, and the intercalation to active material is also accompanied by diffusion polarization. This response can be in the order of minutes to hours.

Therefore, it is preferable to speak about internal impedance than resistance and to consider the impedance spectrum (i.e. impedance module and phase versus frequency) as an appropriate way to get an insight onto these various polarizations. Its evolution with ageing can be a very effective qualitative health indicator[5][6]. It may even, under certain conditions, allow prediction of the battery behaviour, at least in the short to medium term[9]. The drawback is that the classical way of measuring it, by the sweeping in frequency of a sine excitation current, is not straightforward to implement on-board. The internal resistance, which can be seen as a reduced image of the impedance, is easier to access and is therefore also a parameter of interest.

4.3.2 Electrochemical impedance spectroscopy (EIS)

In a Li-ion battery, the charge and discharge mechanism relies on several electronic and ionic processes for successful operation. These processes occur across a range of timescales from picoseconds to minutes and hours. By analysing the response of a battery to voltage or current with respect to time (or frequency of excitation), the behaviour of some of these processes can be separated and understood individually. In EIS, this is done by studying the output impedance signal from an applied sinusoidal current or voltage. The phase shift and magnitude of the output signal can then be used to determine the impedance.

Different internal mechanisms inside the battery can be linked to specific time domains and hence respond to specific excitation frequencies. By altering the frequency of the input current or voltage and investigating how the resulting phase shift (and impedance) changes with input frequency, the relationship between individual mechanisms and their individual impedances can be isolated and understood.

As a battery ages the performance characteristics alter. The process governing these performance characteristics can be traced back to changes in the internal electrochemical mechanisms. These changes (and the mechanisms responsible for them) can be observed via the changing impedance vs. frequency relationship with lifetime.

Typically, these results are displayed in a Nyquist plot where the impedance is separated into the real and imaginary components and the two components plotted on the X and Y axis respectively, as shown in Figure 2.

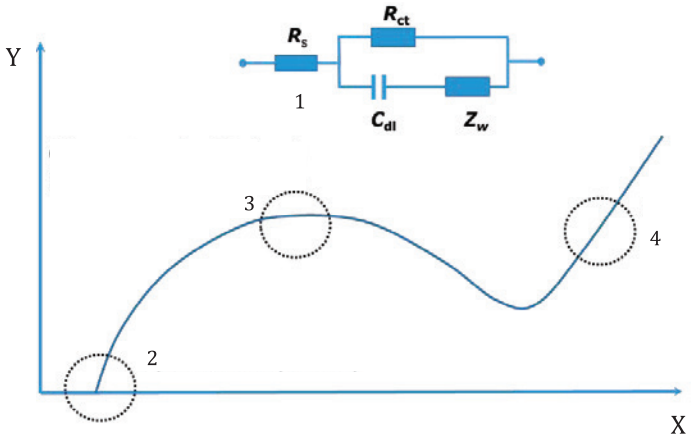

Key

X real (Z), mΩ
Y imaginary (Z), mΩ
1 equivalent circuit
2 ohmic resistance (R_s) 0 phase shift (i.e. DC)
3 charge transfer (R_{ct}) and double layer (C_{dl}) region, Hz
4 Warburg impedance (Z_w) solid state diffusion region, mHz

Figure 2 — Schematic of a Nyquist impedance plot

The key attributes of the battery can then be observed, and an equivalent circuit can be used to map the attributes to the physical behaviour inside the battery. Figure 3 illustrates schematically.

Over time these attributes may change. This may be due to several factors such as;

— the introduction of surface layers, slowing down to electrolyte /electrode transfer, increasing resistance;

— poorer electrical connection between the electrode particles, increasing the electrical resistance;

— loss of surface area through pore clogging reducing etc.

Theoretically changes in the battery can be traced through changing impedance spectrum. The behaviour of the EIS spectrum is translated to changes in the individual elements in an equivalent circuit and characterized at each stage throughout the life of the battery.

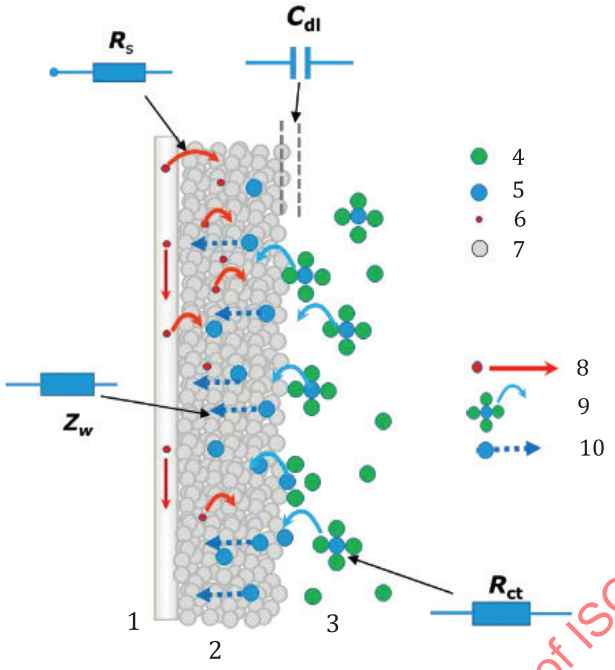

Key

1	current collector	6	electron
2	electrode	7	electrode particle
3	electrolyte	8	electron movement
4	electrolyte molecule	9	Li^+ charge transfer
5	Li^+ ion	10	Li^+ diffusion

Figure 3 — Cell reaction processes and their corresponding equivalent circuit element

In reality there is still some debate about some of the features observed in battery impedance spectra and their physical meaning (e.g. magnitude of specific contributions from surface layer mechanisms at the solid electrolyte interface). It can also be challenging to directly link an equivalent circuit based on impedance spectrum alone to observable charge and discharge behaviour at spacecraft level in Figure 4. For this reason, EIS is primarily used as a powerful tool to qualitatively assess changes in battery but seldom used for quantitative modelling of battery behaviour over life.

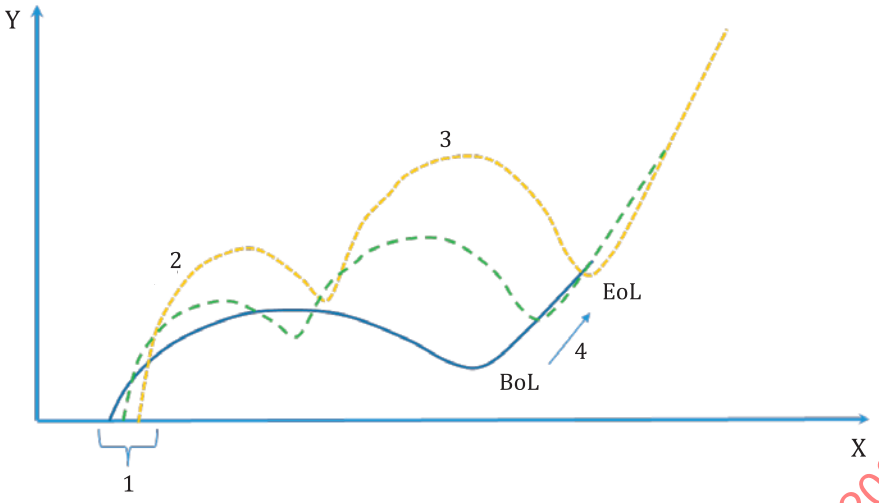

Key

X real (Z), mΩ
Y imaginary (Z), mΩ
1 increasing ohmic resistance
2 introduction surface layer process
3 changing charge transfer resistance
4 ageing

Figure 4 — Schematic of charge state of Nyquist plot with time

4.4 Battery internal resistance

The battery internal resistance is commonly defined by the classic Kirchhoff relationship, with the resistance equal to the ratio of change in battery voltage to change in current that produced it. As mentioned in 4.3, the battery not being a pure resistor, the resistance measure is dependent on the timeframe of measurement; an instantaneous sampling of the change of voltage yields the resistance associated with the fastest mechanisms of resistances (electronic) while sampling over the course of seconds shows the additional contributions from charge transfer and diffusion mechanisms. Extending the resistance sampling time also sees the voltage change as a function of SoC (as per Formulae (2) and (4)). Thus, the measured value obviously depends on the delay between the current change and the voltage sampling. This is illustrated by Figure 5, which shows how large the difference between the values of a cell internal resistance measured by two different methods during the same cycle can be.

R_{int} via the ESTBC method is resistance determined by voltage drop with constant low load.

R_{int} via supplier method is determined by the voltage drop at the end of a higher magnitude current pulse.

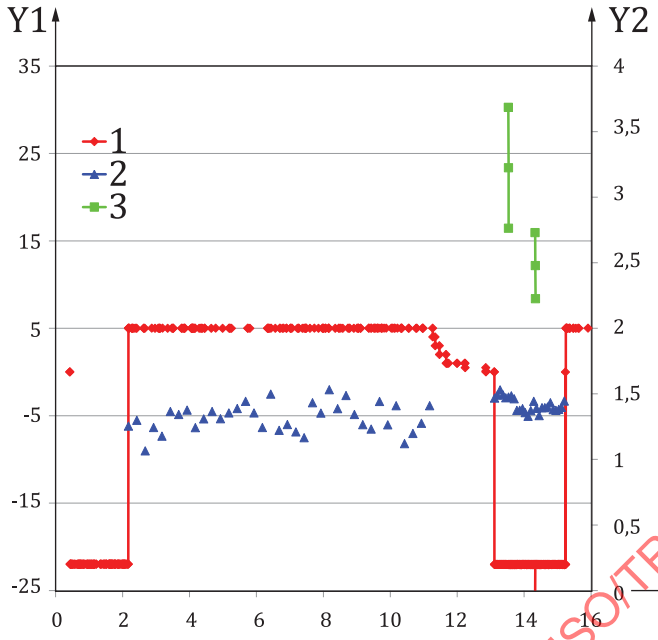

Key

X time (s)
Y1 cell current (A)
Y2 cell internal resistance (Ω)
1 cell current
2 R_{int}, ESBTC method
3 R_{int}, supplier method

Figure 5 — Cell internal resistance, cell current at various state of charge, according to two different methods

The various contributors to the impedance having different time constants, one is consistent in the choice of the sampling delay in order to ensure that the measured value is representative of the actual ageing. Figure 6 shows the evolution with time of the same cell internal resistance measured with these two methods: not only their values but also their evolution with ageing are markedly different (due to the specific resistance mechanisms that the two different techniques capture and how these change over time).

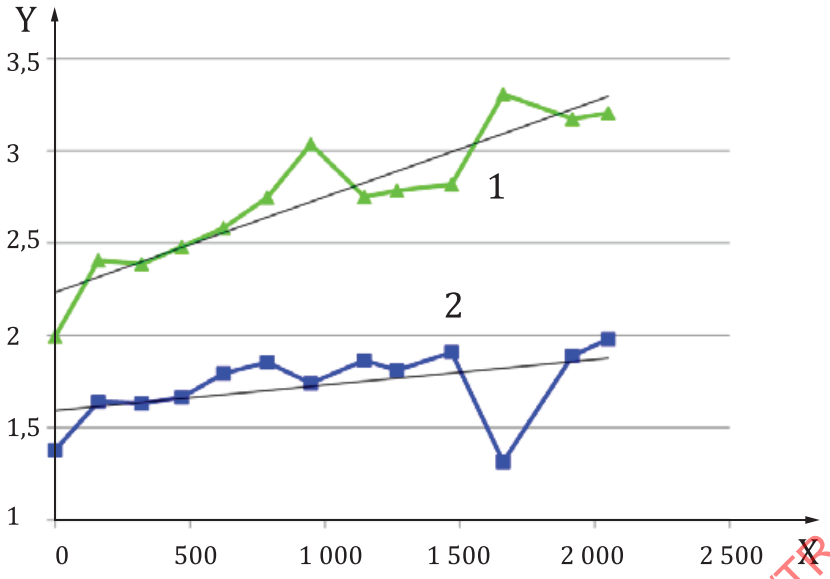

Key

X cycle number
Y resistance (Ω)
1 pulse discharge method
2 constant load method

Figure 6 — Comparative evolution of internal resistance with ageing according to the two different measurement methods of Figure 5 (arbitrary units)

Despite its limitations, the battery internal resistance (measured consistently) can sometimes be the best indicator of the health status of a battery. Indeed, it can occur, with some technologies and under certain operating conditions, that the capacity does not change much during mission life (e.g. to excess capacity of the electrode the most prone to degradation) while in the meantime the internal resistance shows a significant evolution.

Figure 7 illustrates this situation for a real time GEO test where the capacity loss is negligible while the internal resistance increases by almost 40 %. In such a case, the internal resistance appears as the key parameter that would allow detecting an abnormal drift well before any impact on the capacity can be evidenced.

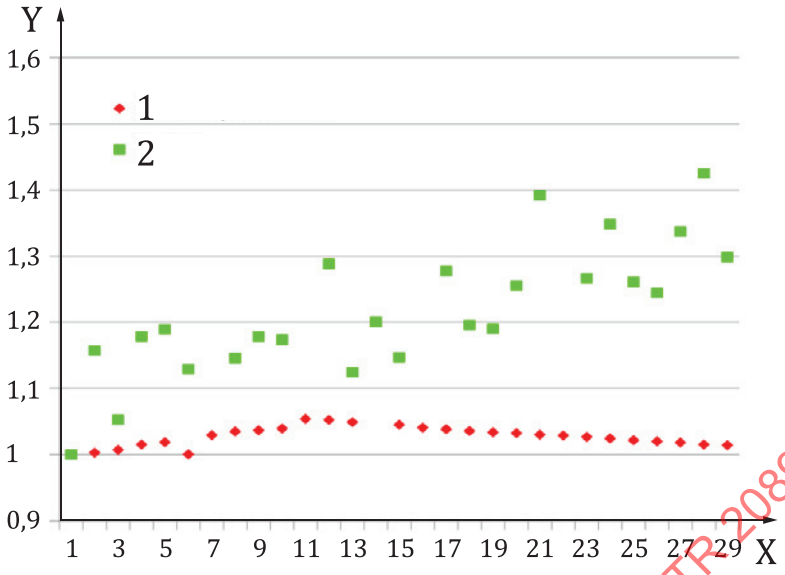

Key

X number of eclipse seasons

Y relative change from BoL (%)

1 C_{meas}/C_{measo}

2 R/R_0

Figure 7 — Relative capacity (red) and internal resistance (green) variations versus eclipse season number in real time GEO cycling

In summary, one or the other of the parameters reflecting the ageing of a battery may be preferred in order to estimate its health status. They are carefully selected and can be accessed individually or globally by direct or indirect methods, which are detailed in Clause 6.

5 Specificities of spacecraft telemetry and resulting limitations

5.1 General

The telemetry implemented on board a spacecraft is primarily aimed at supporting the nominal and contingency operations, not at providing high accuracy/frequency acquisitions nor accurate timing in view of more "technological" needs. Therefore, it is important to be aware of its specificities and limitations.

5.2 Signal digitization

In the most usual implementation, analogue parameters are fed to an ADC that associates a digital value coded on a defined number of bits to an input voltage in a range between zero and full scale. For instance, a 0 V to 5,10 V input range can be coded on 8 bits (i.e. from 0 to 255), providing a quantization step of 20 mV. This quantization is the first source of uncertainty for the measured parameter. For the example ADC, it amounts to approximately 0,4 % of full scale.

In order to make a given parameter compatible with the ADC input voltage range, this one has usually to be conditioned. For a voltage outside of the ADC range this can be done very simply by a resistive divider: in the present example, a divider ratio of 1:8 would offer a range of 0 V to 41 V, adequate for the measurement of a battery voltage operating on a typical satellite power bus (i.e. below 40 V).

For currents, an active circuit is needed to amplify the (usually small) voltage drop present at the terminals of a measurement shunt. Here, for a voltage drop of e.g. 100 mV full scale, an amplification factor of 51 would be necessary. A peculiarity of the battery current is its bi-directionality, while most

often the ADC is single supplied. As a consequence, the charge and discharge currents are usually measured through the same shunt but conditioned via two different chains of opposite gain signs, which transfer functions that cannot be perfectly matched. This can be an issue when trying to access e.g. the round trip efficiency of the battery, which plays on small differences between the measurements of charged and discharged energy.

5.3 Temperature

Temperature can be acquired via thermistors or platinum sensors. The latter is polarized by a current and the voltage at its terminals to be shifted and amplified to fit with the ADC input range. For a thermistor the conditioning is usually performed by making a resistive divider of the thermistor and of a fixed series resistor whose value is equal to that of the sensor in the centre of the temperature range. Supplied at a voltage equal to the top of the ADC range, their common point is directly fed to the ADC. This is usually the case for batteries.

Whatever the parameter and the conditioning applied, the end to end transfer function from the physical value (in volts, amps or degrees) to its digital representation throughout the useful range needs to be established. This takes the form of a "calibration curve" and can be given as a series of points in between which a linear interpolation can be performed or by a polynomial of a certain degree obtained by a best fit to measured data, etc. In all cases this introduces a certain level of uncertainty, of different impact depending on the nature and range of the parameter.

5.4 Voltage

For the battery voltage, the relative variation between EoC and EoD is rather small; the useful range is only a limited fraction of the full scale and therefore the quantization effect is more visible. In turn, the calibration can be optimized for this relatively small voltage extend.

5.5 Current

The current can spread the whole range from zero to full scale, both in charge and discharge. Considering again the example of the round trip efficiency, the amount of charged energy during the final phase of taper is very sensitive to any offset of the telemetry chain in the vicinity of zero current. Figure 8 shows a taper charge phase observed in flight. The offset, around 60 mA, is not insignificant and it is worth observing that, after a quite long duration of taper, where the current is almost flat, i.e. in reality equal to zero, the telemetry drops down to zero only at the beginning of discharge, when the ADC saturates low.

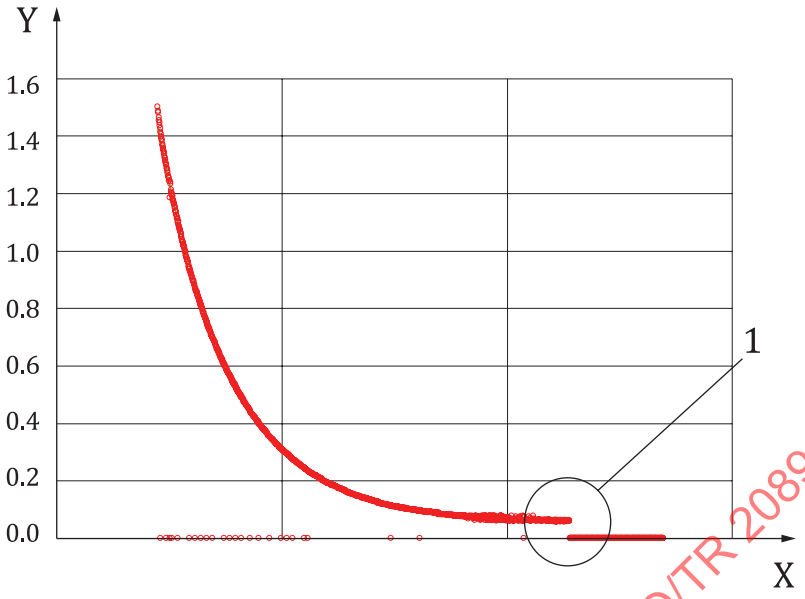

Key

X time (arb units)

Y current (A)

1 beginning of discharge, ADC saturates low

Figure 8 — Current profile observed via spacecraft telemetry chain showing offset

5.6 Sampling frequency

The acquisition rate can also be a potential concern when having to, for example, detect the trespassing of a given threshold or to integrate current. For the former an interpolation is necessary while the latter may experiment an uncertainty attached to the ratio of the sampling interval to the duration of the integration. As an example, a 20 seconds sampling period on a 30 minute eclipse would introduce, in the worst case, up to 2 % error. Again, in the round trip efficiency case, this is far from negligible w.r.t. an energy loss of less than 10 %.

Fortunately, many spacecraft have a so-called dwell mode, allowing a faster sampling of selected parameters for a period of time. It is common to achieve a rate of one to a few tens of hertz.

5.7 Synchronisation

Another critical aspect is the timing of the acquisitions of several parameters. Depending on the telemetry chain design, it can be that the sampling of two parameters is separated by a duration that is significant in regard of the sampling period. When observing e.g. the battery current/voltage behaviour during a transient, such a lack of synchronization is an obvious issue.

5.8 On-board memory

Last, many spacecraft in LEO do not store on board the complete set of telemetry data acquired in between to communication sessions with their ground control station. The data set can be limited to, e.g. a sub-sampling of the parameters plus the minimum and maximum recorded during the period. Obviously, this makes any sort of fine processing very challenging.

7.3 provides a number of recommendations aimed at increasing the usability of the data acquired via the spacecraft telemetry chain.

6 Main methods for the evaluation of battery ageing parameters

6.1 Global method: fitting of a numerical model to in-flight data

6.1.1 General

To characterize the changing SoH of a battery a classic approach is to fit an existing numerical model of the system to in-flight data. In principle this approach gives access to all the battery parameters (e.g. capacity, internal resistance, diffusion), within the model representativeness and accuracy.

6.1.2 Model structure

Most often a numerical model of a flown battery or, indeed, of the cells making it, is available, from either the battery supplier or the spacecraft manufacturer, chiefly for design purposes. Such models can be based on various structures.

A number of very classical topology are shown in Figure 9. They are made of a number of discrete electrical components (voltage sources, resistors, capacitors, etc.) which together represent the observable behaviour of the cell from the electrical point of view. They are often referred to as the "black box" model, since they do not intend to reflect the internal electrochemical and physical behaviour of the cell.

The values of the components depend on the ageing and on the instantaneous operating conditions (temperature, SoC, current, voltage, etc.). The mathematical functions describing their dependence onto the operating conditions can be more or less complex, according to the needed degree of representativeness, accuracy and timescale.

Another class of models aims at representing, down to a variable level of details, the internal electrical and electrochemical behaviour of the cell. As an example, the model shown in Figure 10 is commonly used at ESA for design verification and in-flight health status assessment, e.g. in view of mission extensions. Being close to the actual cell construction, it is able to reproduce its behaviour down to relatively small time scales.

Other models do not attempt at reproducing the internal or external cell behaviour by discrete or (semi) continuous electrical elements but come under the form of pure mathematical descriptions. These can be the transcription, in a form that can be processed by a computer, of the theoretical formulae of electricity, electrochemistry, chemical kinetics and more. The variety of these models is large.

A last type of models is made of the purely empirical ones. There, the operating point of a cell under given conditions is interpolated inside a data base built from tests performed in a variety of settings. The main drawback of this approach is the need for a large data base, meaning a lot of testing and resulting into high cost and long duration. It is seldom used, since building a model of the previous type requests far less effort.

The cell behaviour being highly temperature dependent, most of the cell numerical models also provide the thermal dissipation as an output, which is fed to the cell or battery thermal model to derive its operating temperature. This aspect is of minor interest here, since the temperature can be read directly from the telemetry, possibly after some corrections due to the actual battery/spacecraft thermal configuration.

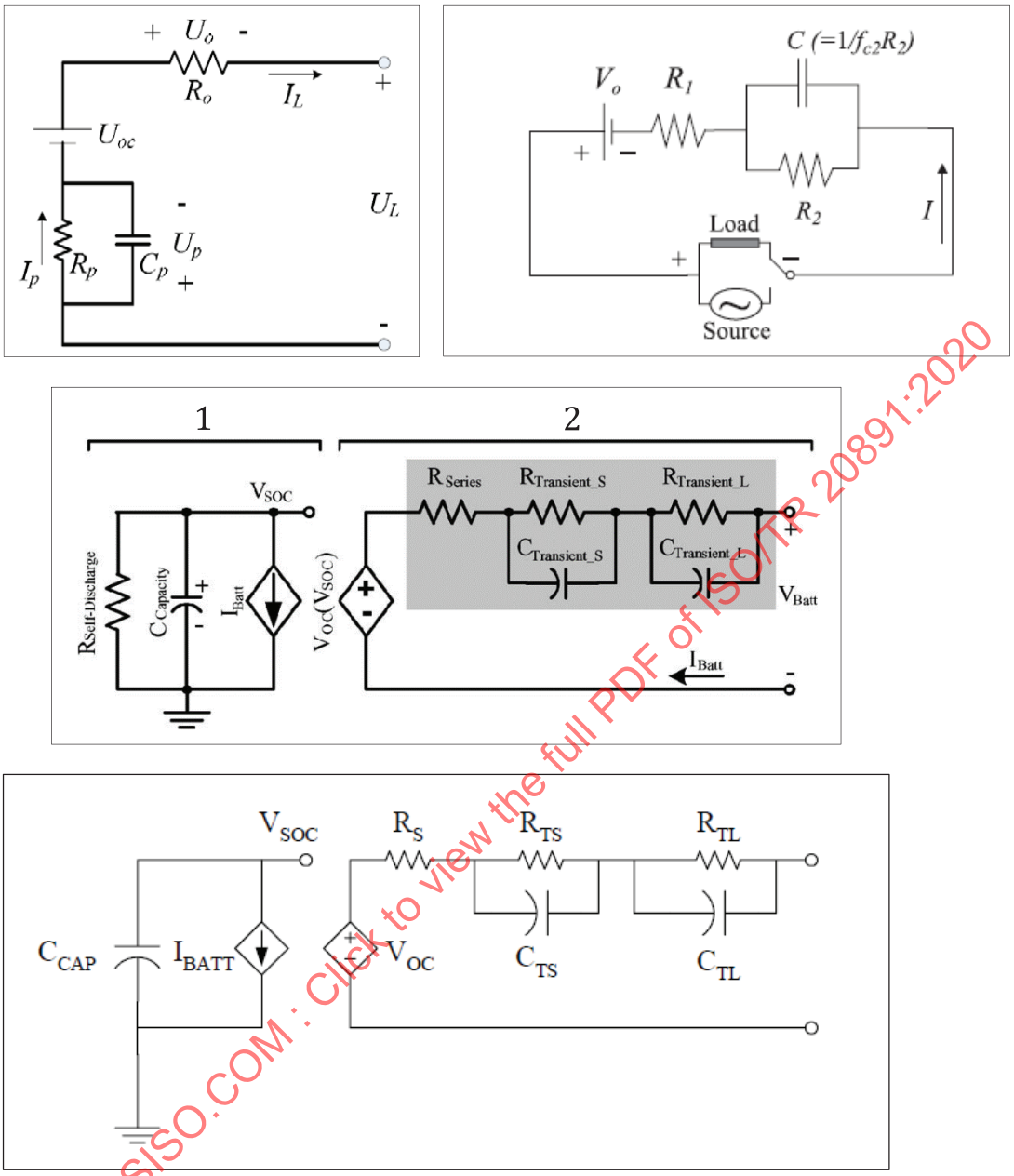

Key

1 battery lifetime

2 voltage-current characteristics

Figure 9 — Upper left, generic Thevenim model; upper right, model by B. Y. Liaw [1]; Middle, model by Chen et al.[2]; bottom, model by Knauff et al.[3]

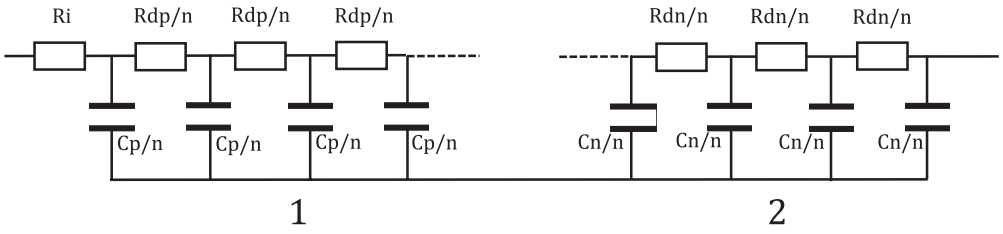

Key

1 positive electrode

2 negative electrode

Figure 10 — G. J. Dudley model[4]

6.1.3 Data fitting

6.1.3.1 General

Whatever the type of model, the exercise of fitting a set of in-flight data assumes the tuning of a number of parameters inside the model; this number can be more or less large, depending on the type of model and its level of detail. In any case it is difficult to ensure that the achieved fit is the best possible and that a different set of values would not provide a better one. Therefore, the significance of a particular set of values can be questioned and, if the values of specific parameters are critical to evaluate the health status of the cell, this introduces some room for uncertainty.

In addition, performing this fitting manually is usually cumbersome. This is why some techniques have been developed in order to make this activity more automatic, as illustrated in Figure 11. There, a Kalman filter (in red) is used to dynamically improve the fitting to the experimental measurements (in blue). One can see that the convergence is very good, making such techniques very attractive in that they would make the health assessment much faster and therefore more easily repeatable, an important point for ensuring a regular follow-on and the building of a meaningful trend analysis.

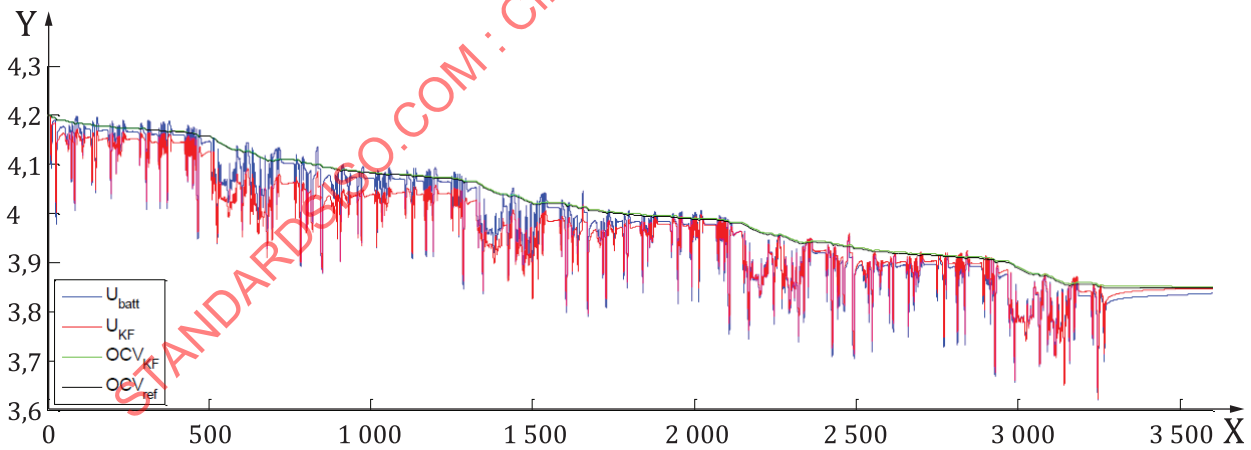

Key

X time (s)

Y voltage (V)

Figure 11 — Battery voltage fitting on electrical vehicle discharge profile (Master thesis, Matthias Kuipers, ISEA, RWTH Aachen University)

An activity under ESA contract was performed by ISEA/RWTH Aachen (Germany) to evaluate the effectiveness of such an approach when applied to actual in-flight telemetry data from two spacecraft on different orbits (Cryosat 2 in low Earth orbit and Mars Express on an elliptical Mars orbit). The activity

focused on the estimation of the available capacity alone, using a parametric cell model developed by ESA. The main outcomes were:

The result can vary significantly, depending on the initial set of parameters introduced into the simulation, due to the existence on many local optima in a space the dimension of which is defined by the number of tunable parameters. In order to assess the error possibly introduced, a set of "synthetic" data was generated using the model itself. In theory, the algorithm should converge to the set of parameters having produced these data; but in practice, this was the case only for a fraction of the simulations performed, many ending in one of the previously mentioned local optima.

Whatever the precautions taken, the estimated capacity is difficult to assess for low depth of discharge cycling, since only a small fraction of the voltage versus DoD curve is explored. In addition the battery is almost never in a steady-state condition, being charged or discharged most of the time. This makes access to the open circuit voltage quite difficult.

The similarity of the successive charge/discharge cycles is relatively high in a spacecraft. This is very visible when comparing Figure 12 to Figure 11. The consequence is that only a limited amount of operating points, within the multi-dimensional space, are available to identify the model.

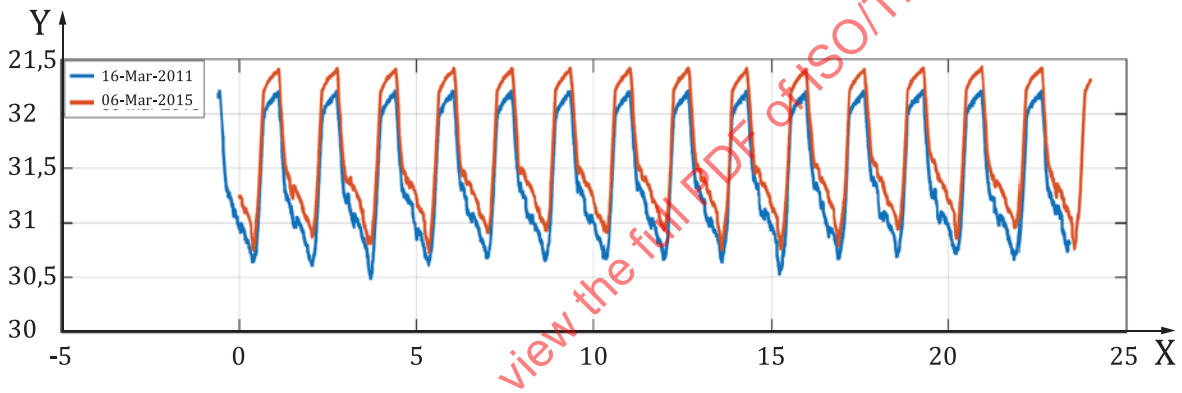

Key

X time (s)

Y voltage (V)

Figure 12 — Mars express battery voltage profile at two different period

Another important aspect is the quality of the available measured data. Obviously, the time resolution, the accuracy of the measurements, their proper time stamping… all play a role in the quality of the final result. In the present case, the temperature plays a specific role, in that it dynamically affects the cell behaviour. Therefore, it is important to know what the temperature in-flight measurement represents: a thermal sensor located on a cell, on the battery baseplate or nearby on the spacecraft wall, will exhibit a temperature less and less representative of the average cell one, which drives the temperature sensitive behaviour of the battery. A dedicated thermal model may be implemented to provide a better estimate of the "real" temperature and thus a more valid input to the fitting process.

Additional aspects as specified in 6.1.3.2 to 6.1.3.5 may be considered for a successful data fitting.

6.1.3.2 Simulation input

In order to do a successful data fitting, a model of the battery (and possibly the control electronics) is simulated with input profiles extracted from telemetry. The following discussion distinguish between two possible options of preparing the simulation input profiles: The first option (i) uses the charge/discharge current from telemetry as a direct input to a simulation of the battery only, while the second option (ii) uses the profile of available charge power and actual discharge power as an input to a simulation of the battery and control electronics including the taper charge logic. The main difference between these two options is which profiles are imposed. In option (i), the SoC profile can be computed directly from the integral of the current profile, the initial SoC and the battery capacity. Thus, the

electrical model is used only to simulate the corresponding voltage. As a consequence, the complete taper charge phase, including the length of the taper charge phase, is imposed based on the telemetry. In option (ii), the taper charge phase is also simulated based on a model of the control electronics. Figure 13 shows a comparison of the consequences of both options on the simulation. The two plots on the left side show the results for option (i) and on the right side for option (ii). For option (i), the currents match perfectly (since it is imposed on the simulation), but the end of charge voltage deviates due to model inaccuracies. For option (ii), the voltages match perfectly during taper charge (since it is a simulation parameter in this case), but the corresponding charge current deviates due to model inaccuracies. For the shown example (telemetry of the SWARM satellites), both options lead to very similar fitting results. The only difference is the implementation of the fitting process, in particular in choosing the initial conditions and the reconstruction of the available charge power as discussed in 6.1.3.3 and 6.1.3.4.

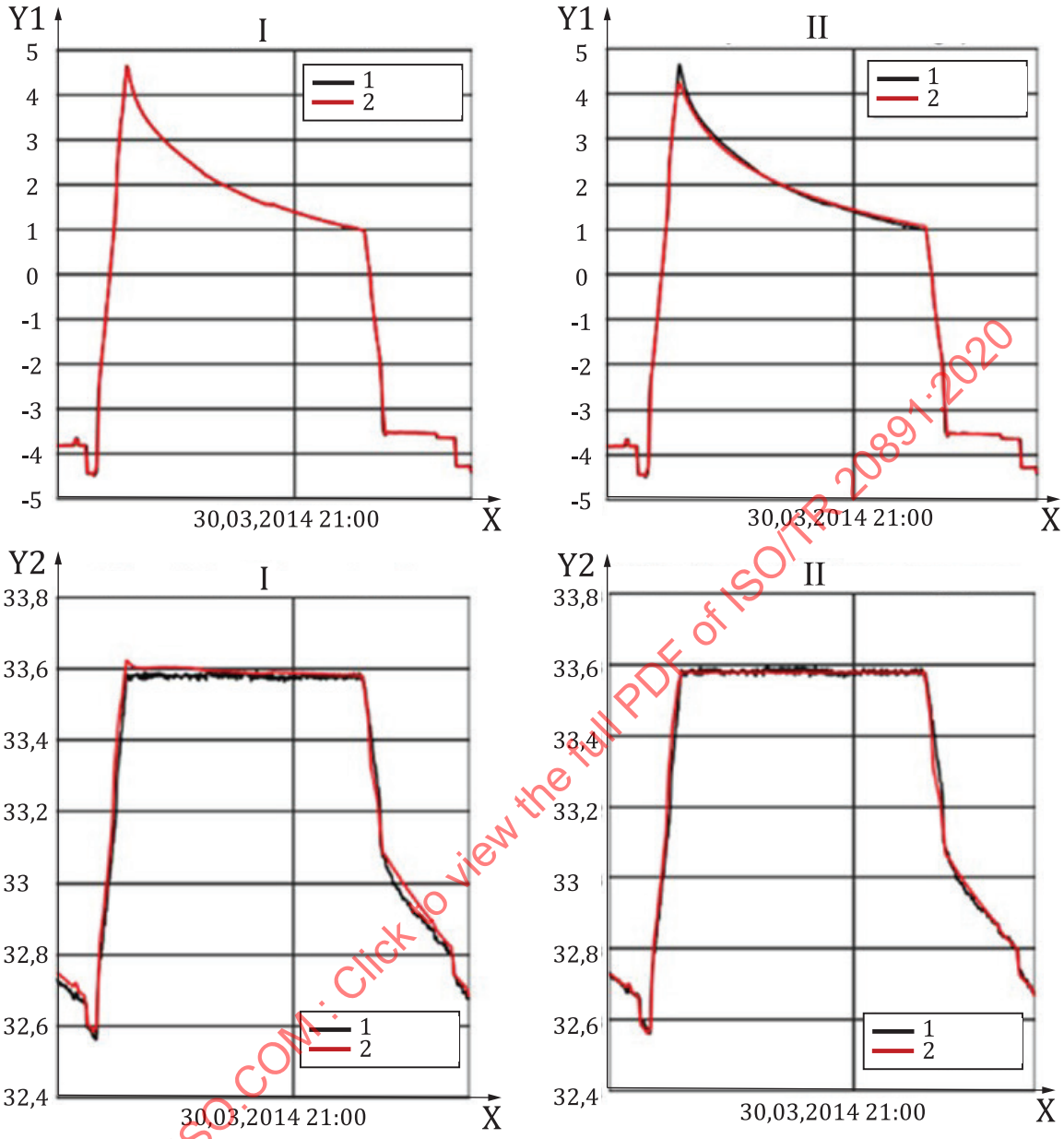

Key

X time
Y1 charge current (A)
Y2 bus voltage (V)
1 telemetry
2 simulation
I simulation with imposed current profile
II simulation of taper with available charge power

Figure 13 — Comparison of simulation options: available charge power vs. imposed current profile

6.1.3.3 Initial conditioning

In general, the unknowns of a simulation-based data fitting are not only the model parameters but also the initial condition of the simulation. Thus either (a) the initial condition is included in the fitting

process as variables to be determined or (b) the simulation is started from an approximated initial guess and the model error is evaluated first after the impact of the initial condition is decayed. However, approach (b) is only possible for a stable simulation over many orbits, which is difficult in combination of option (i) discussed in 6.1.3.2. For long simulations, the accumulated error in the integral of the current profile leads to a drift of the SoC profile. Thus, simulating only the battery according to option (i) usually needs the initial SoC to be fitted as an additional unknown parameter. Figure 14 shows an example of the decay of a biased initial SoC for a full simulation according to option (ii) in 6.1.3.2 for the example of a simulation-based fitting of a satellite on a drifting LEO with a body mounted solar array. The initial SoC for an interval of telemetry data is approximated by a simplified model of the battery voltage and total equivalent resistance at begin of life and from the bus voltage and battery current taken from the first sample of the telemetry data. For the iterative fitting of the degradation parameters, the first orbits are ignored in order to skip the convergence from the inaccurate initial condition.

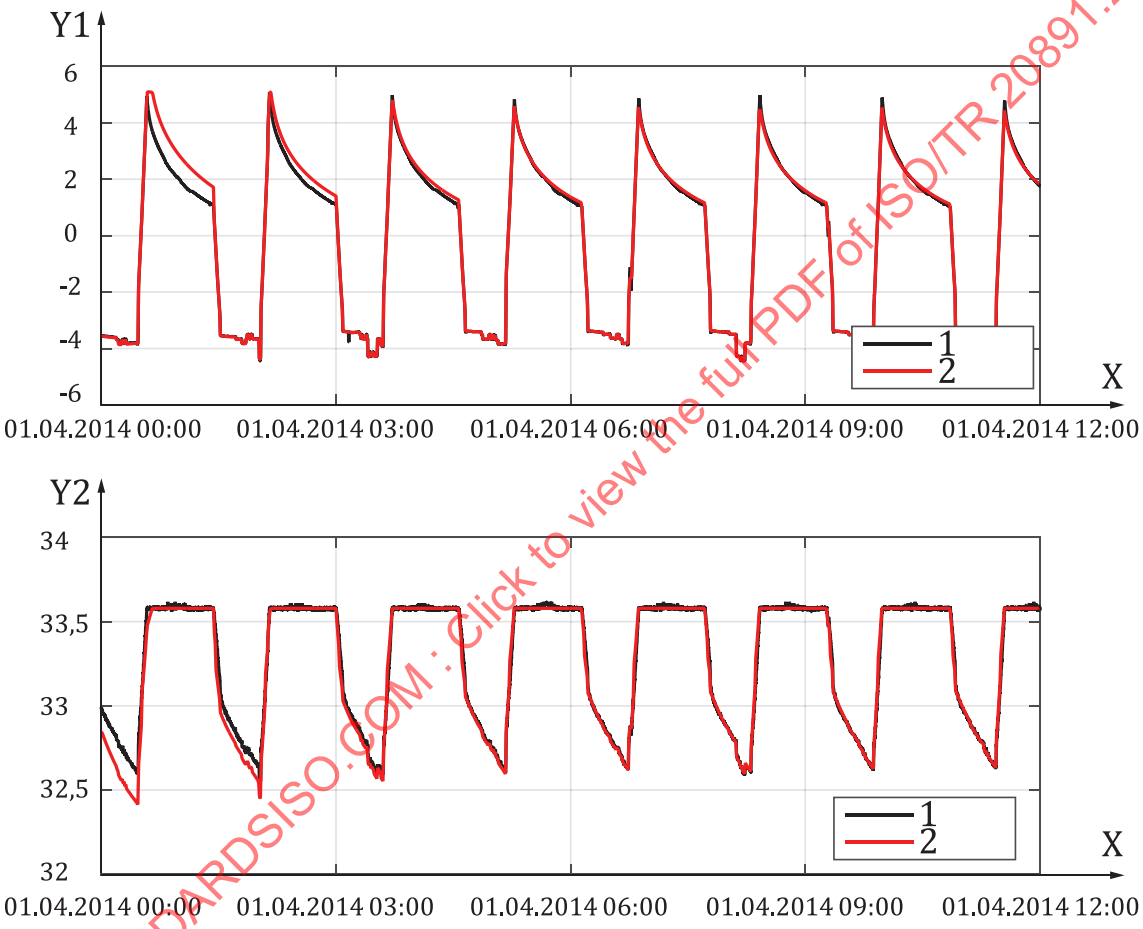

Key

X time
Y1 charge current (A)
Y2 bus voltage (V)
1 telemetry
2 simulation

Figure 14 — Decay of unknown initial condition for simulation-based data fitting

6.1.3.4 Available charge power

For a simulation according to option (ii) in 6.1.3.2, the profile of the available battery charge and discharge power is necessary. For fitting to in-orbit data, these profiles are extracted from the

spacecraft telemetry. However, for the charge phase, the telemetry includes only the actual charge power, which is already reduced due to the spacecraft on-board regulation (limiting charge current or end of charge voltage). For a stationary profile (same SoC before and after one orbit), the integral of the charge/discharge power yields exactly the dissipated energy of the real battery. Simulating this data with a battery model with slightly higher losses lead to an unstable simulation due to a negative energy balance. This behaviour complicates the iterative search for the best model parameters during the fitting process. Therefore, it is beneficial to simulate the complete control loop and use the available charge power instead of the actual charge power, i.e. the maximum available power provided by the primary energy source (e.g. solar generator). Thus, the actual charge power is an output of the simulation whereas the input is the available charge power. This enables a stable simulation also with model parameters leading to higher losses than observed in the telemetry data. Overestimating the losses still leads to a deviation of the voltage profiles between simulation and telemetry, which is considered by the parameter fitting. But allowing this overestimation helps stabilizing the overall fitting process, which updates the parameters from iteration to iteration in order to find the best correlation with telemetry. Figure 15 shows an example of the reconstructed charge power for a satellite with body mounted solar array and a long taper charge phase, leading to a reduced power profile in the telemetry. Since the satellite uses a power point tracker for solar array regulation, it is difficult to reconstruct the realistic available primary power from telemetry only. Therefore, a simplified approximation is utilized of just holding the available charge power during taper charge on the last value before entering the taper charge phase. The resulting rectangular profile of the available charge power does not reflect the real available energy per orbit but enables the simulation of a taper charge phase independent of the telemetry.

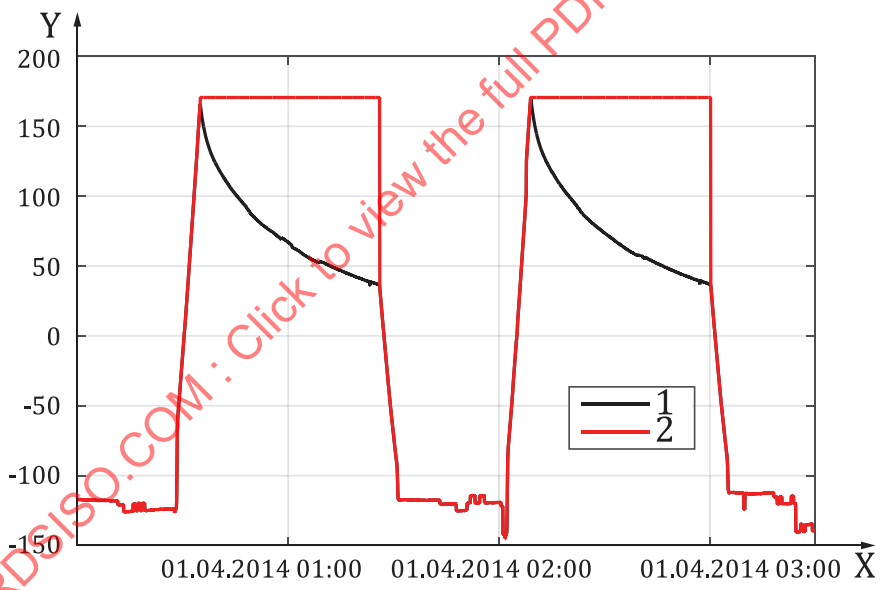

Key

X time
Y battery charge power (W)
1 telemetry
2 simulation input

Figure 15 — Reconstructed charge power used as simulation input

6.1.3.5 Weighting of an objective function

In general, the simulation model may not be fitted perfectly to the telemetry data even with an optimum parameter set due to inaccuracies in the telemetry data or physical effects, which are not covered by the simulation model. Therefore, it is beneficial to weight the evaluation of the model error in order to focus

onto the phases where a good correlation is expected. The lower plot of Figure 16 shows an example of a weighting function which implements the following fitting conditions:

— ignoring the first 10 orbits in order to skip the convergence from inaccurate initial conditions (only necessary if the initial SoC is not included as an unknown in the fitting process according to approach (b) in 6.1.3.3);

— focusing the fitting to the discharge phase (only applicable for option (ii) in 6.1.3.2, where the end of charge voltage is a known model parameter);

— suppressing errors introduced by slight time shifts by exclusion of fast transients at transitions from charge to discharge and vice versa;

— reducing weighting at the beginning of the discharge phase to reduce the impact of inaccuracies in modelling the transient chemical processes.

Figure 17 shows the results of assessing the battery performance with the presented fitting technique on the example of the SWARM spacecraft with body mounted solar arrays on a LEO with drifting ascending node.

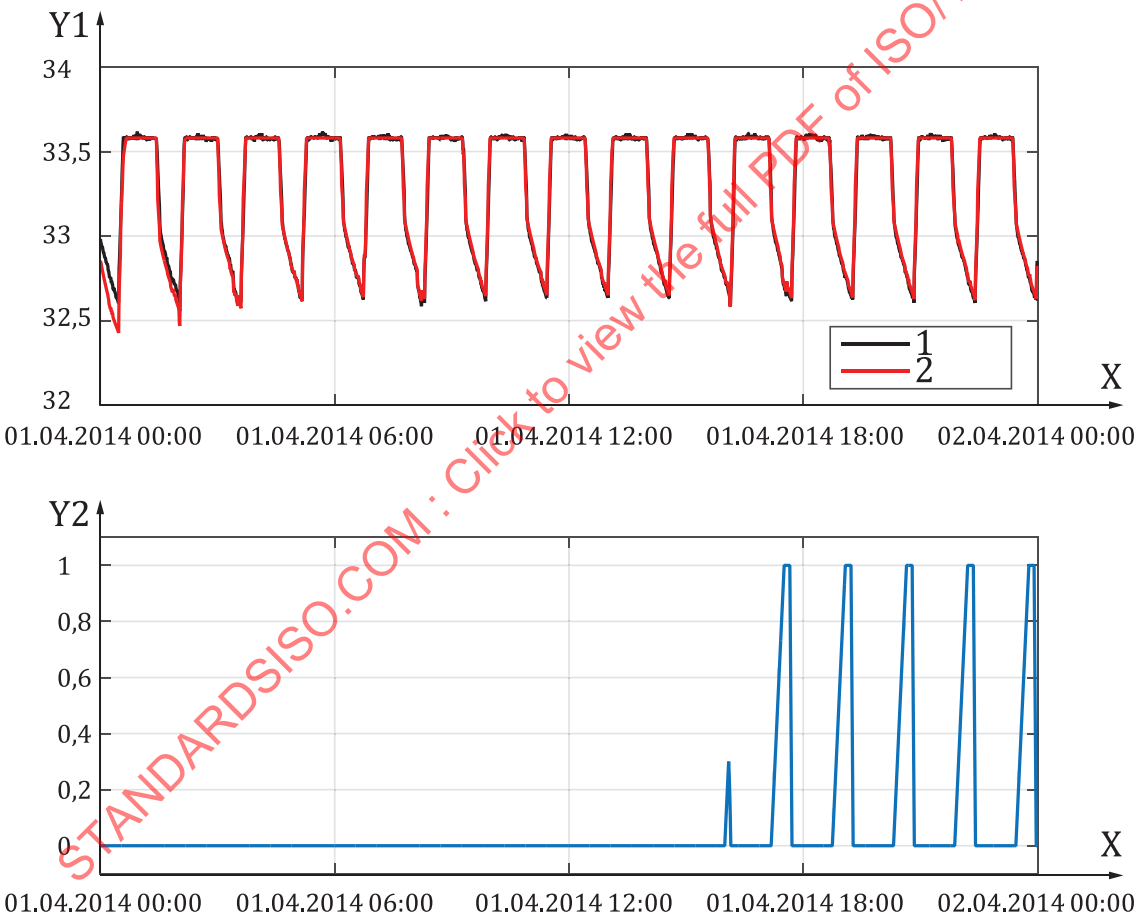

Key

X time
Y1 bus voltage (V)
Y2 weighting function
1 telemetry
2 simulation

Figure 16 — Example of a weighting function used for error evaluation

The whole fitting process, including repeated simulations (as shown in Figure 16) in order to reach correlation of the voltage profiles, is applied to each day of the telemetry data, leading to an estimate of the capacity fade over time. The eclipse length shown in the middle subplot of Figure 17 varies over time due to the drift of the orbit plane. For eclipses shorter than 25 minutes, the depth of discharge of the battery is too small in order get a reliable estimation of the battery parameters. For example, for phases with no eclipse, the battery isn't used at all. Therefore, the processing is limited to telemetry intervals with eclipse lengths longer than 25 minutes.

The only free parameter used in the fitting process is the capacity fade of the battery, where the increase of the battery internal resistance is considered by a fixed ratio w.r.t. the capacity fade. The lower plot of Figure 17 shows the time profile of the fitted capacity fade. The plot reveals that the estimation is biased by the commanded EoCV configured within the spacecraft regulation loop (see upper plot of Figure 17). The EoCV was reduced from 33,6 V to 32,2 V in May 2014, after commissioning was completed and the power subsystem was considered to be stable even with a lower EoCV. Thus, after May 2014, the battery is operated on a lower stationary SoC profile than before, where the estimation of the capacity fade with the presented technique of data fitting yields different results.

In order to reach a good correlation between telemetry data and simulation, the capacity fade can even be set to negative values after May 2014, corresponding to a higher battery capacity than considered begin of life. These results lead to the assumption, that the used model does not cover all contributing components and therefore the absolute values of the estimated capacity fade are necessary to be interpreted carefully. However, the relative evolution of the estimated capacity fade provides information about the battery degradation over time. The black dashed line in the plot of the estimated capacity fade in bottom of Figure 17 shows the linear regression of the values after May 2014 (after switching to 32,2 V EoCV) and only for orbits with an eclipse length longer than 35,5 minutes, which serves as a trend estimation of the capacity fade.

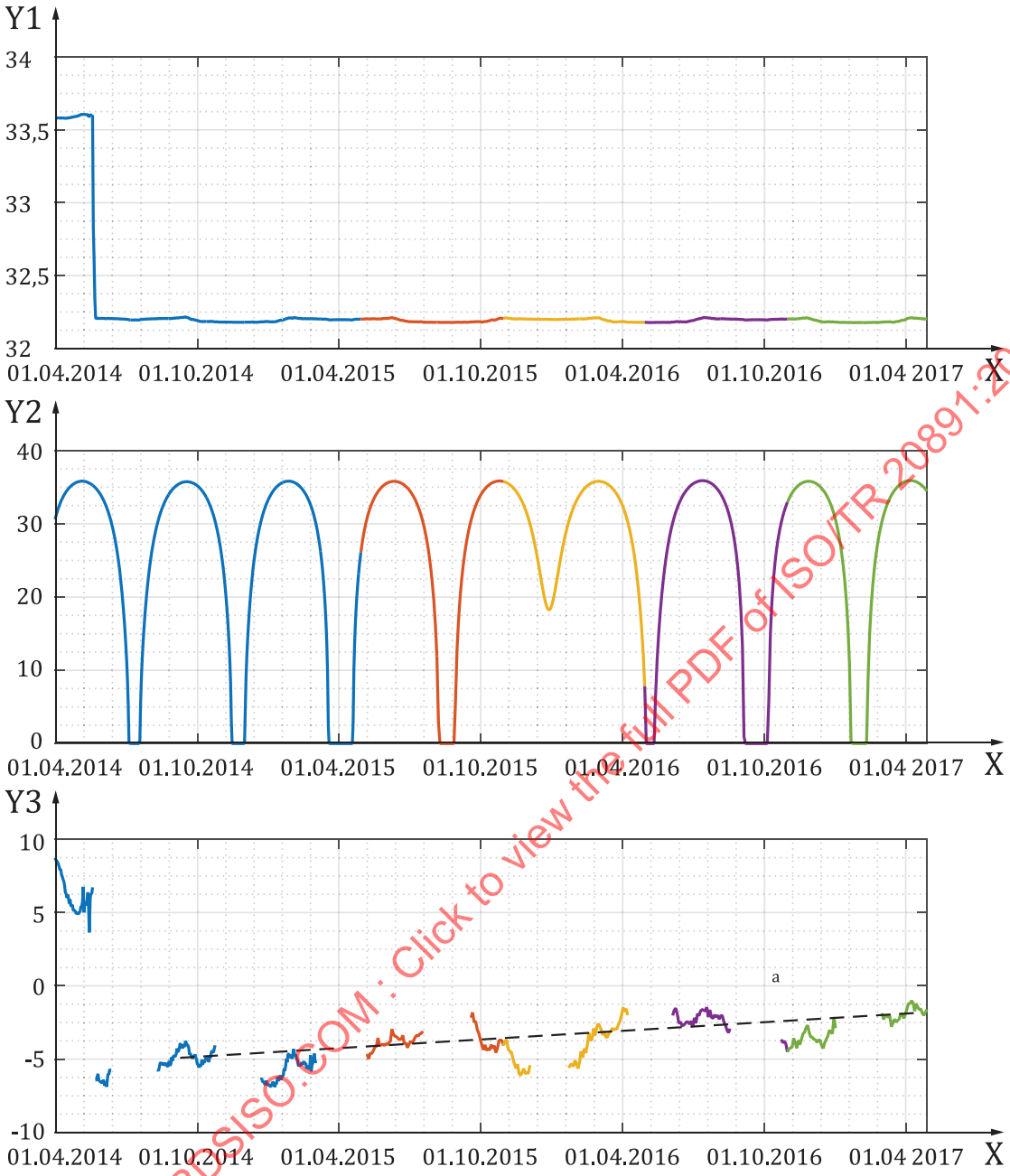

Key

X date
Y1 EoCV (V)
Y2 eclipse length (min)
Y3 estimated capacity fade (%)
[a] 1,2 % per year.

Figure 17 — Results of fitting capacity fade to telemetry data of the SWARM satellite

6.2 Evaluation of battery capacity

6.2.1 Direct method

The calculation is based on the SoC/EMF dependency as shown in Figure 18 and on the following assumptions:

— During taper charge mode (constant voltage at bus level), the current decays exponentially. This assumption holds only for long enough taper charge phases, when the transient behaviour due to chemical diffusion becomes second order and for a linear SoC/EMF dependency, which is a good approximation for EMF above 32 V during the final approach to the EoCV.

— The voltage at the time when the battery current crosses zero after discharge represents the EMF at the EoD.

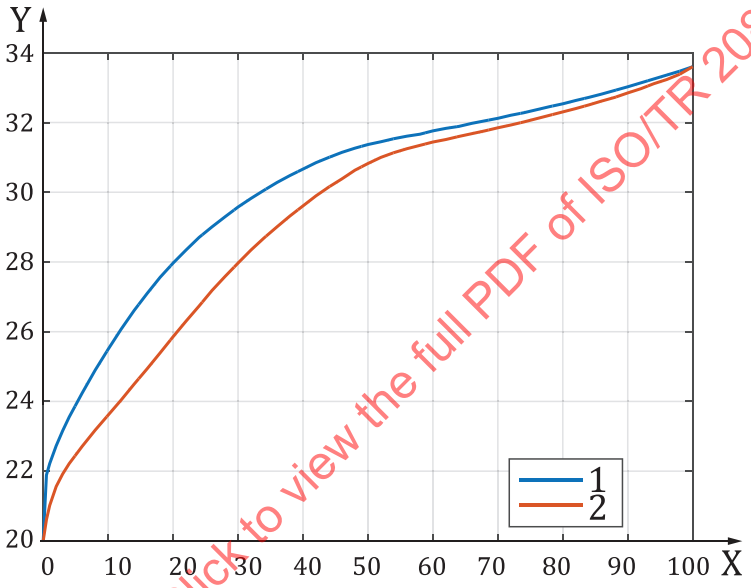

Key

X SoC (%)
Y EMF (V)
1 charge
2 discharge

Figure 18 — SoC/EMF dependency

The calculation of the capacity can be described with the example shown in Figure 19 (telemetry data on 01.04.2014 from 00h00 to 05h00).

For each orbit, the capacity is calculated from the discharge phase starting at the end of the taper charge phase t_{EoC} (blue marker in the plot) and ending at the positive zero crossing of the battery current t_{EoD} (red marker in the plot). The total charge drawn from the battery during this interval is calculated by the integral of the battery current:

$$\Delta Q_{\mathrm{dischage}} - \int_{t_{\mathrm{EoC}}}^{t_{\mathrm{EoD}}} I_{\mathrm{bat}}\, dt \tag{5}$$

Separately, the EoC voltage V_{EOC} and the EoD voltage V_{EOD} are extracted from the measured bus voltages at V_{EOC} and V_{EOD} (respectively blue and red marker in the lower plot of Figure 19). For both voltages, the

corresponding SoC is determined from the charge and discharge curves of the SoC/EMF dependency shown above and the SoC difference is calculated by:

$$\Delta S_{SoC} = S_{SoC}(V_{EoC}) - S_{SoC}(V_{EoD}) \quad (6)$$

This difference corresponds to a discharge of the battery starting from a state of full charge at V_{EOC}. In reality, the taper charge is interrupted by the eclipse before the EMF reaches V_{EOC}. The missing amount of charge is estimated from an exponential function, fitted to the battery current during the final 15 minutes of the taper charge phase. The fitting is a linear regression in the natural logarithmic space of the battery current and is shown in Figure 19 by the solid red curve for the fitted interval and the dashed red curve for the extrapolation. The missing charge to reach the EoCV is therefore equal to the integral of the dashed red curve from t_{EoC} to infinity.

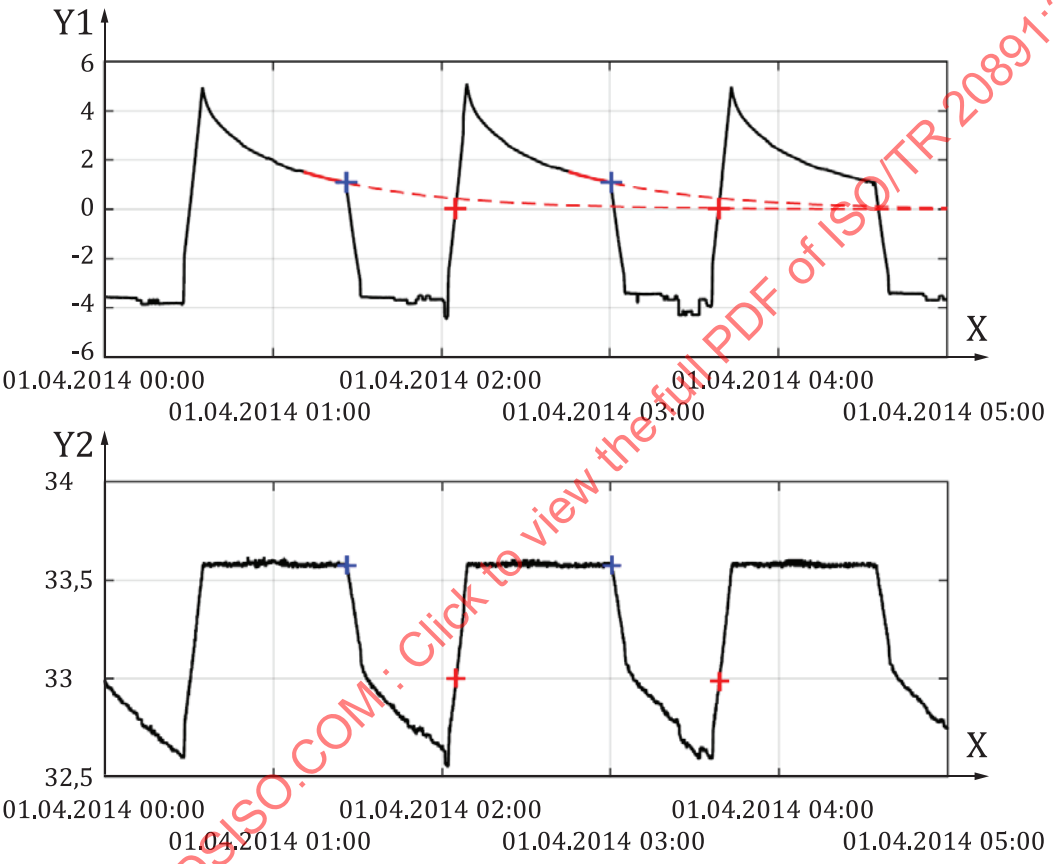

Key

X time
Y1 battery current (A)
Y2 bus voltage (V)

Figure 19 — Example of direct calculation of capacity fade by current fitting.

The equivalent battery capacity from full charge is therefore given by:

$$\Delta Q_{\text{bat, EoL}} = \frac{\Delta Q_{\text{discharge}} + \Delta Q_{\text{missing taper}}}{\Delta S_{\text{SoC}}} \tag{7}$$

And the relative capacity fade is defined by the capacity reduction w.r.t. the nameplate capacity:

$$f_{\text{capacity}} = \frac{Q_{\text{bat, BoL}} - Q_{\text{bat, EoL}}}{Q_{\text{bat, BoL}}} \tag{8}$$

Figure 20 shows the results of the presented approach. In order to evidence a trend in battery capacity fade, the calculation was made for all orbits at least 30 minutes long and a daily average calculated as the median value of all orbits during each day, which is then plotted versus the date. Figure 20 contains the following three plots (each curve is separated into three-time intervals corresponding to different mission periods).

— profile of the EoCV, calculated as the average of the measured bus voltage during taper charge phases;

— profile of the eclipse duration;

— result of the estimated capacity fade.

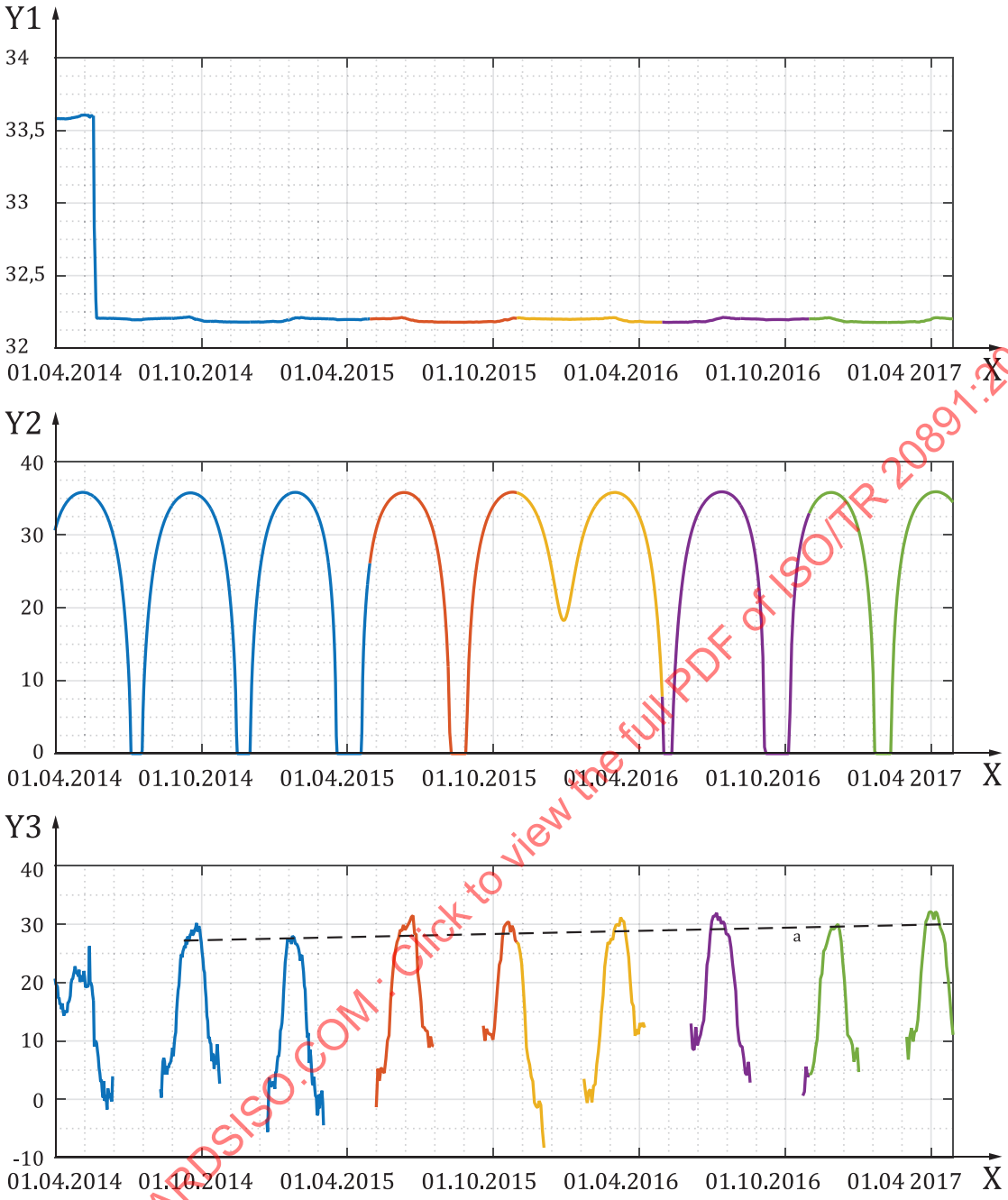

Key

X date
Y1 EoCV (V)
Y2 eclipse length (min)
Y3 estimated capacity fade (%)
[a] 1,1 % per year.

Figure 20 — Results of the capacity fade estimate for the SWARM satellite

The results are clearly difficult to interpret and the influence of e.g. the change in EoC voltage is not explained. Even if a trend of approximately 1 % per year can be built on these eclipses lasting at least 35,5 minutes (i.e. the one of the "flat" parts of the curves), this needs to be taken with precaution. It is worth noting that the trend estimation provides similar results compared to the comprehensive data fitting as presented in Figure 21. Both results are based on telemetry of the same satellite.

This methodology has also been applied to ground testing carried out by China Aerospace Science Corporation (CASC) as can be seen in Figure 21, which describes the fitting of the taper charge curve with an exponential function to determine the remaining capacity.

Using this methodology, the data from ground test cycling under a representative load for 4 years was compared.

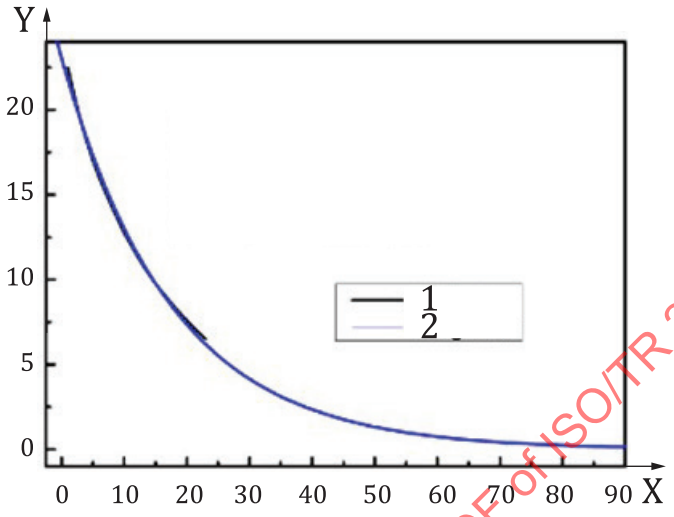

Key

X time (s)
Y current (A)
1 initial data
2 fitting data

Figure 21 — Exponential fitting used to determine remaining capacity after taper charge completion

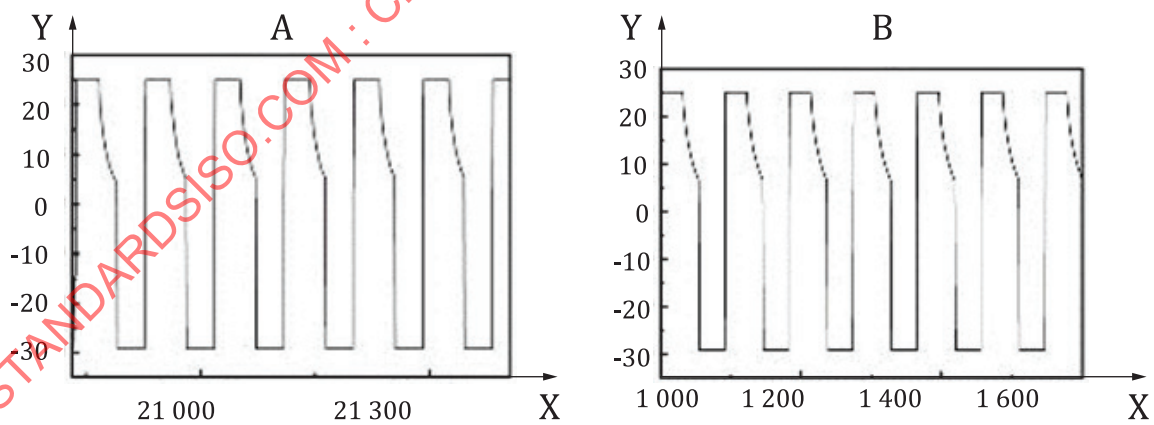

Key

X time (min)
Y current (A)
A test at t_0
B test at t_0+4 years

Figure 22 — Current profile (including taper charge) of electrical cycle of satellite battery ground test

Using the technique described in Figure 21 and applying it to the cycling data from Figure 22, the available capacity vs. time can be plotted. In Figure 23, the results can clearly be seen of the diminishing capacity with cycle number; interestingly the EoDV displays a similar downward trend but it does not perfectly match the capacity loss; this is due to other factors (such as SoC-dependent resistance) affecting the voltage, suggesting that care should be taken when selecting which metric to use for state of health measurement.

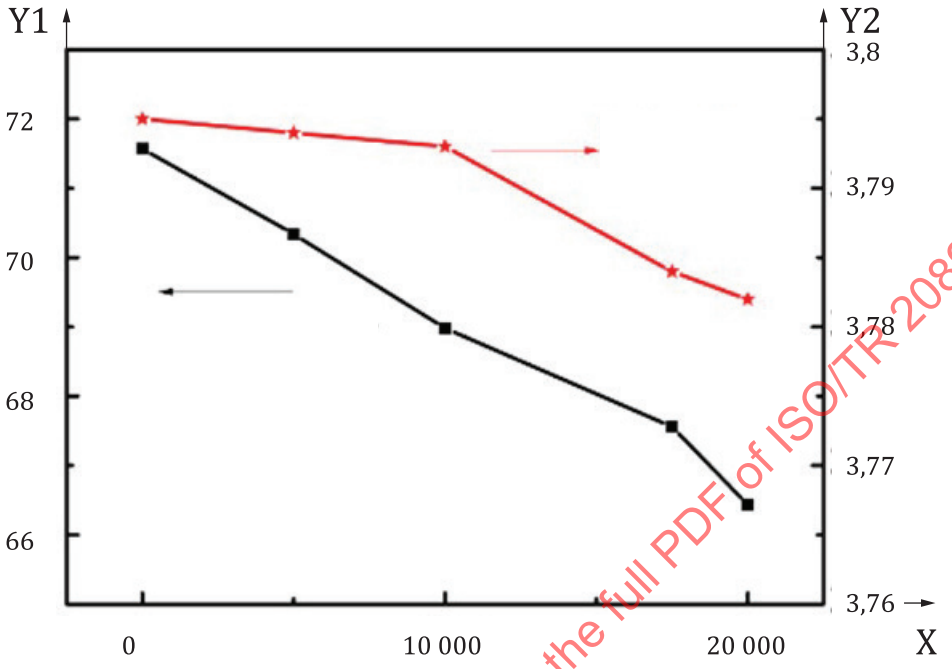

Key

X cycle number
Y1 capacity (Ah)
Y2 voltage (V)

Figure 23 — Capacity fade during 20 % DoD cycling over 20 000 cycles vs. change in EODV

6.2.2 Indirect method

Eddahech et al.[5] have used the constant voltage part of a classical CC/CV charging process to derive a relationship between the time constant of the current decay and the loss of capacity during a calendar ageing test. Figure 24 shows a result achieved for an NCA type of cell, where the correlation is excellent.

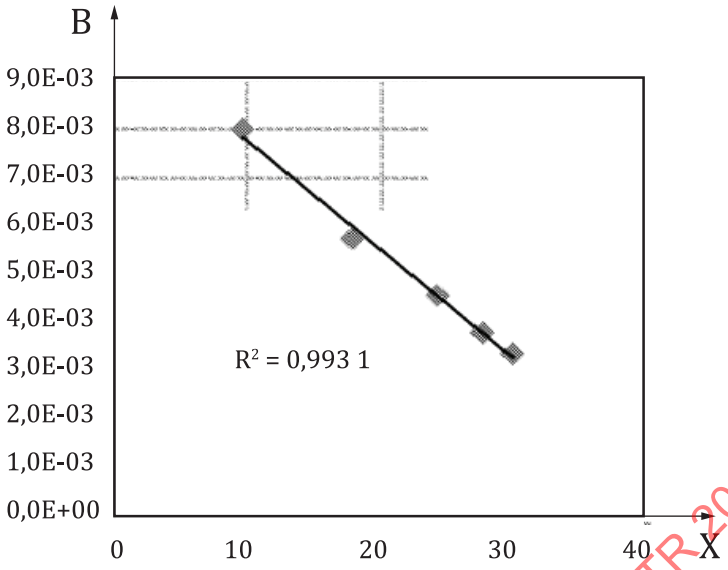

Key

X capacity loss (%)

Figure 24 — Exponential coefficient of the current decay during CV charging phase versus capacity loss[5]

Such a result suggests that, provided a preliminary calibration is made beforehand, the capacity loss can be quite accurately derived from the examination of the CV charge phase. A major interest of this method is that the coefficient of the exponential decay of the current during this phase is obtained by curve fitting of the current measurement versus time. Therefore, the telemetry limitations of a satellite are of limited consequences, (a) because the charge current resolution is quite good in view of the explored range of values and (b) because the noise and other sources of uncertainties are "filtered" by the fitting process.

The relationship is probably not always as linear as illustrated in Figure 24, as depicted by Figure 25, where the same relationship is shown for the same NCA type of cell, this time during a real time LEO cycling test. The difference in ageing mode may play a role. However, the range of capacity loss in this last case is smaller than for Reference [5] and it might be that the function becomes more linear at higher degradation. The range of the B coefficient is different, confirming the need for prior calibration.

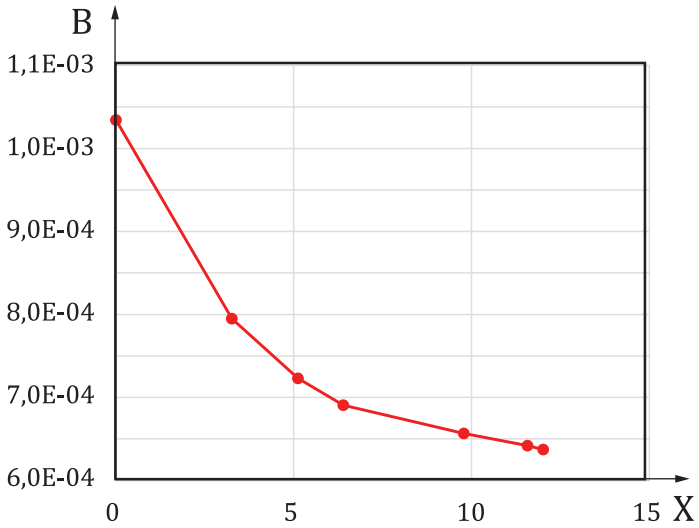

Key

X capacity loss (%)

Figure 25 — Exponential coefficient of the current decay during CV charging phase versus capacity loss[5]

6.3 Measurement of battery internal resistance

6.3.1 Direct internal resistance measurement

The direct in-flight measurement of the battery internal resistance uses the same principle as applied on ground, i.e. observing the change in voltage resulting from a current step. Such steps occur naturally as a consequence of the spacecraft operation (units switch on/off…) or can be forced for the purpose of the measurement (i.e. switch on/off of heaters for a short duration in eclipse).

The main difficulty of this method lies in the necessary accuracy of the current and voltage measurements. The voltage is of specific concern, since the battery low internal resistance and the limited amplitude of the current transient result in a very small voltage step, usually not much larger than the telemetry resolution.

A way to circumvent this difficulty is to process a large number of uncorrelated events to reduce the effect of telemetry quantization, provided that the electrical power system architecture offers this possibility. Figure 26 shows the result of this approach in the specific case of a spacecraft which battery is directly connected to the bus and its taper charge voltage regulated by the switching of solar generator sections under computer control at 1 Hz. The thermal control being itself independently operated at 2,5 Hz, the result is an almost permanent unbalance of the solar array and load current and therefore the battery is constantly charged or discharged, the average current staying null. The linear fitting of the voltage versus current is very good, as shown by the R^2 larger than 0,99, and the slope gives directly the battery internal resistance, here 59,5 mΩ.

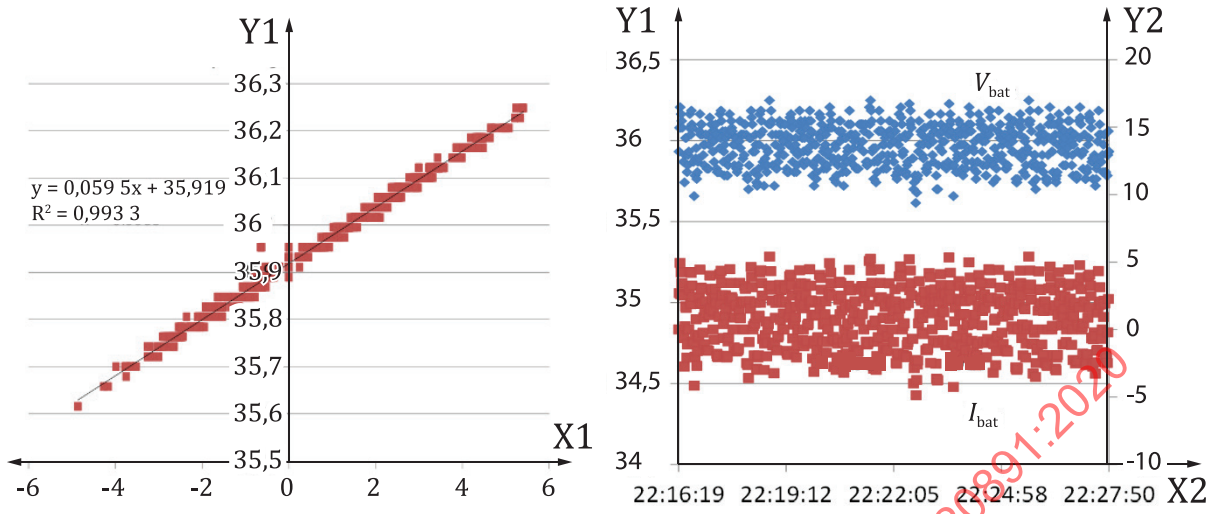

Key

X1 current (A)
X2 time (h:m:s)
Y1 voltage (V)
Y2 current (A)

Figure 26 — Computer controlled taper charge: battery voltage versus current fitting (left), battery current and voltage vs time (right)

A further approach was also applied to the same spacecraft, this time using eclipse data of the same orbit. There, the principle is to smooth the discharge voltage versus time curve by removing the ohmic drop, i.e. tuning the internal resistance to get the best fit of a polynomial trend curve to the data points. The result is visible in Figure 27, where the curve is approximated by a 6th order polynomial. The best fit is achieved for an internal resistance value of 55,2 mΩ. This is reasonably consistent with the previously mentioned 59,5 mΩ one, given the quite different battery operating conditions.

The main issue with resistance measurement is its sensitivity to the actual current step amplitude and sampling delay, which are usually different in-flight from the ones applied e.g. at unit acceptance testing. This comes directly from the difference in time constant of the various phenomena implied and may render difficult the interpretation of in-flight results, if not previously correlated on ground.

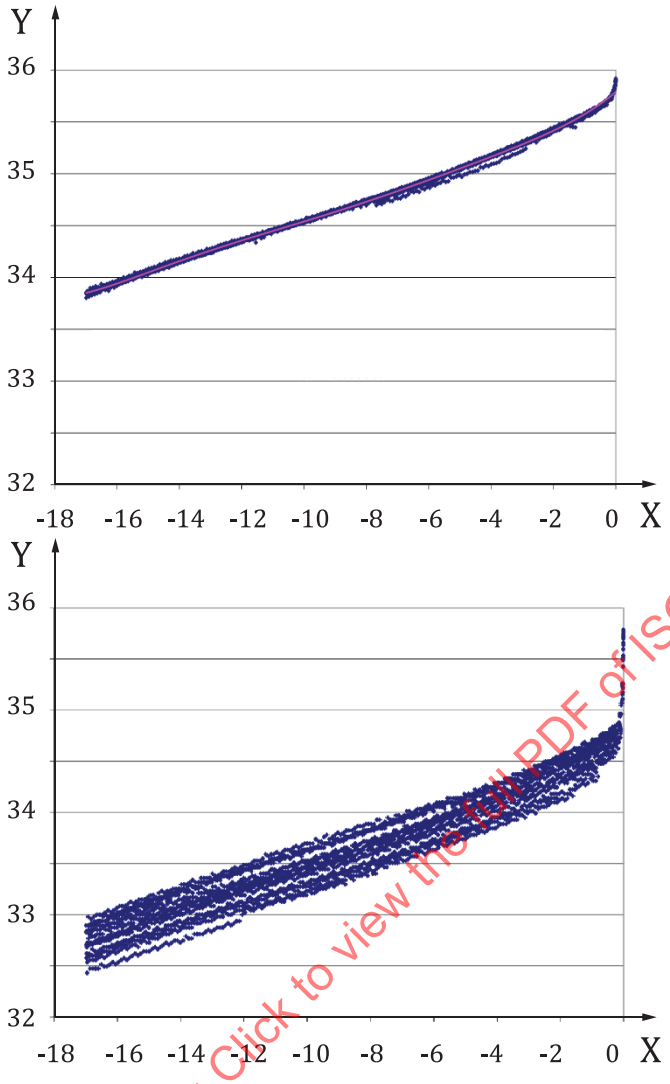

Key

X current (A)

Y voltage (V)

Figure 27 — Battery voltage versus removed charge (negative) during eclipse; top figure, raw data, bottom figure, data after removal of the ohmic voltage drop

6.3.2 Indirect measurement of battery resistance

6.3.2.1 General

The direct measurement of the battery internal resistance is not always possible, e.g. due to limitations of the spacecraft telemetry or unfavourable operating conditions. In such a case, some methods that provide an indirect estimation of the internal resistance can be of help.

6.3.2.2 Constant current / constant voltage (CC/CV) charging phase processing

During the CC/CV charging of a battery, the first phase (constant current) sees the battery voltage increasing under the accumulation of the charging current, while the second one (constant voltage) sees this current decaying more or less exponentially, a behaviour resembling the charging of a capacitor in series with a resistor under similar conditions.

Based on this analogy, a parameter having the dimension of a capacitance C can be identified from the CC phase by:

$$C = I_{ch} \frac{\Delta t}{\Delta V} \tag{9}$$

where

I_{ch} is the charging current;

Δt is a time interval;

ΔV is the battery voltage change during Δt.

Similarly, the product of this capacitance by the series resistance, assimilated to the battery internal resistance, has the dimension of a time constant, which can be identified from the decay of the current versus time. The following example illustrates this approach.

The voltage and current versus time are shown in Figure 28, and the capacitance derived from Formula (1) for the CC phase are shown in Figure 29. The result is very poor, the noise on current and voltage having a huge impact on the result, as is usually the case when calculating derivatives. In order to improve the situation, both are replaced by a trend curve (i.e. a constant value for the current and a 6th order polynomial for the voltage). Figure 30 shows the almost perfect voltage fit and Figure 31 the resulting capacitance estimate, which varies with time since the voltage vs. time curve under constant current charging is not linear.

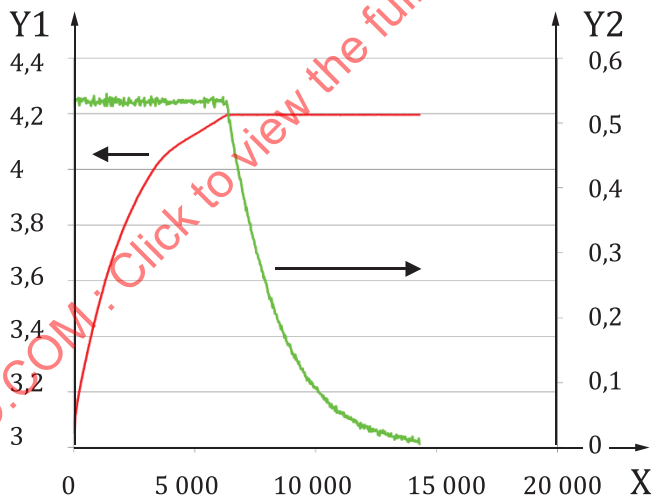

Key

X time (s)
Y1 voltage (V)
Y2 current (A)

Figure 28 — Battery voltage and current in charge.

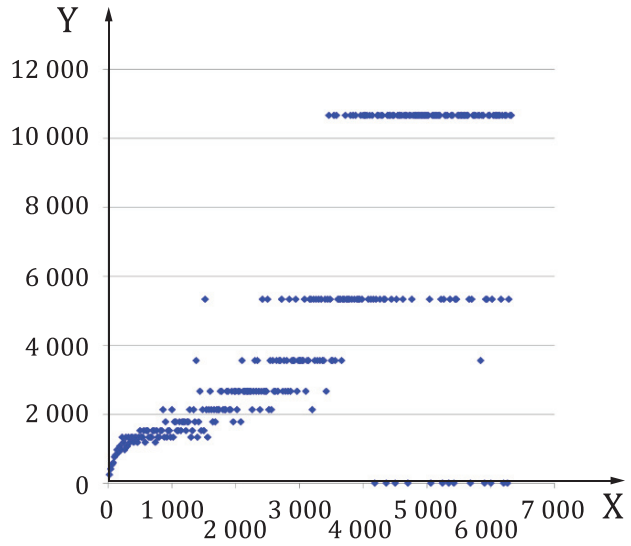

Key

X time (s)

Y capacitance (F)

Figure 29 — Estimated capacitance

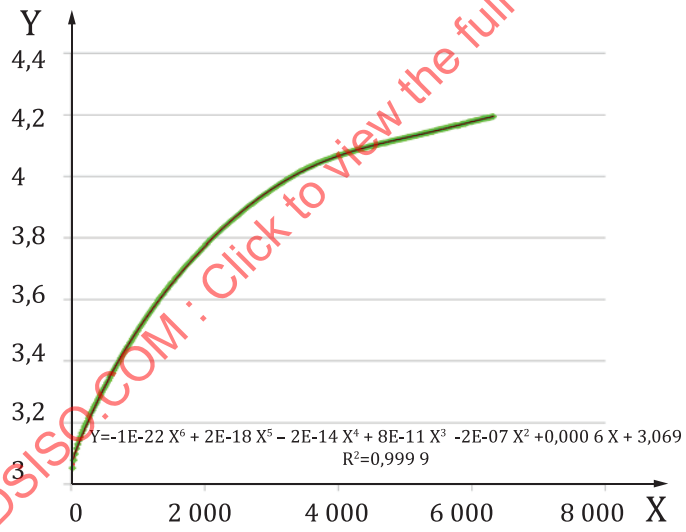

Key

X time (s)

Y voltage (V)

Figure 30 — Voltage noise removal

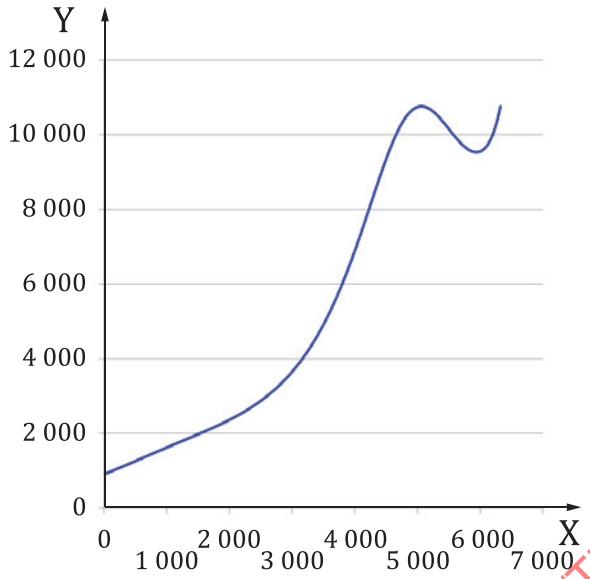

Key

X time (s)

Y capacitance (F)

Figure 31 — Voltage noise removal

The fitting of the decaying current during the CV phase is shown in Figure 32 and is visibly very good. The value of the time constant is 2 095 s. Dividing this value by the capacitance estimated above (close to 10 750 F at end of CC phase) gives a value for the resistance of approximately 195 mΩ. The direct measurement of the cell internal resistance at 100 % SoC was 178,4 mΩ.

In this specific case, this indirect method seems to provide a valid estimation of the internal resistance.

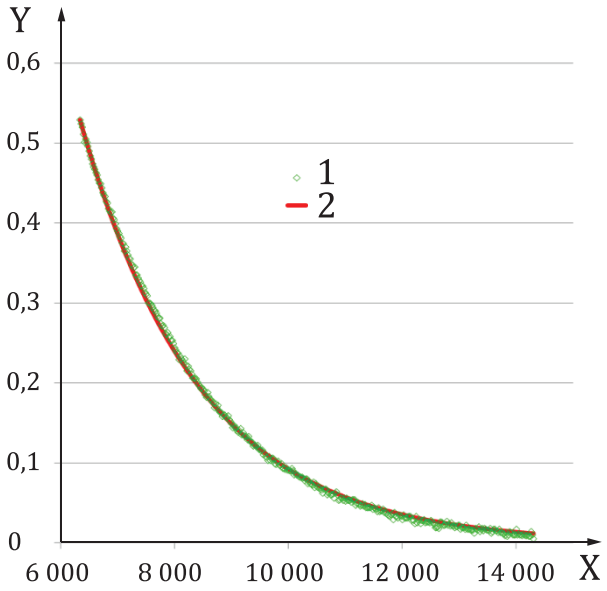

Key

X time (s)
Y current (A)
1 measurement
2 RC fit

Figure 32 — Fitting of the decaying current during CV charging phase

However, the results are not always as satisfactory. Table 1 summarizes results from 5 different types of cells and it can be seen that the above case (#1 in Table 1) is more the exception than the rule. Again, this is not unexpected, since there is no reason for which the identified "internal resistance" would match the result of a direct measurement, whose value depends strongly, among others, on when the voltage has been sampled after the current change.

Table 1 — Results of indirect method for internal resistance measurement versus actual values charging phase

Cell type	Capacitance from CC phase (F)	RC from CV phase (s)	RC/C (mΩ)	Measured Rint (mΩ)
Type #1	10 750	2 095	195	178,4
Type #2	2 476	837	338	400,5
Type #3	5 473	2 159	395	170,3
Type #4	11 318	3 673	324	286,5
Type #5	30 272	1 258	41,5	6,4

This does not make this method useless, though. In fact, as shown in Figure 33, the relative evolution of the internal resistance can be quite well identified, even if the absolute value derived from the indirect method does not match the actual one (this result has been established on cell type #5).

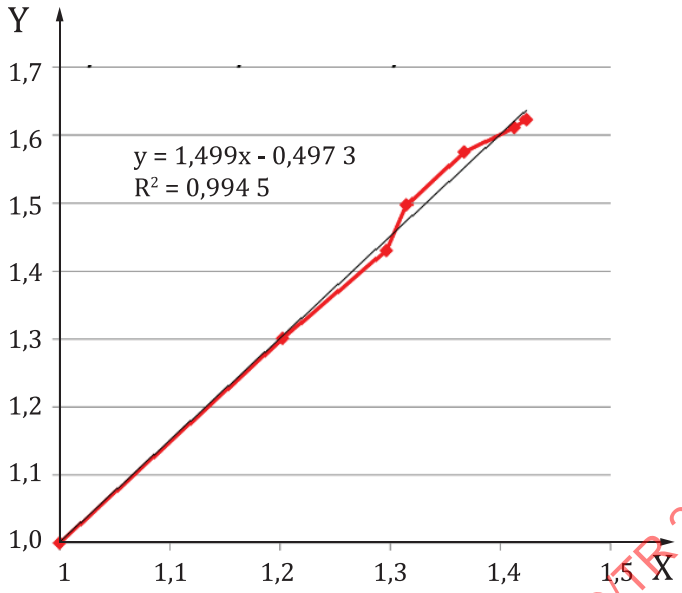

Key

X relative increase of internal resistance from measurement

Y relative increase of internal resistance from CC/CV

Figure 33 — Relative evolution of internal resistance derived from CC/CV phase vs. the same from direct measurement

Another source of uncertainty is the way the battery taper phase is managed either during ground testing or in flight. At least three different approaches are commonly used as illustrated in Figure 34:

— regulated taper, i.e. the battery voltage is actually regulated by the spacecraft power conditioning functions; this is applied to most spacecraft where the battery is directly connected to the bus;

— reduction of the charging current by steps of fixed value each time the battery voltage reaches the EoC voltage;

— reduction of the charging current by a given factor each time the battery voltage reaches the EoC voltage.

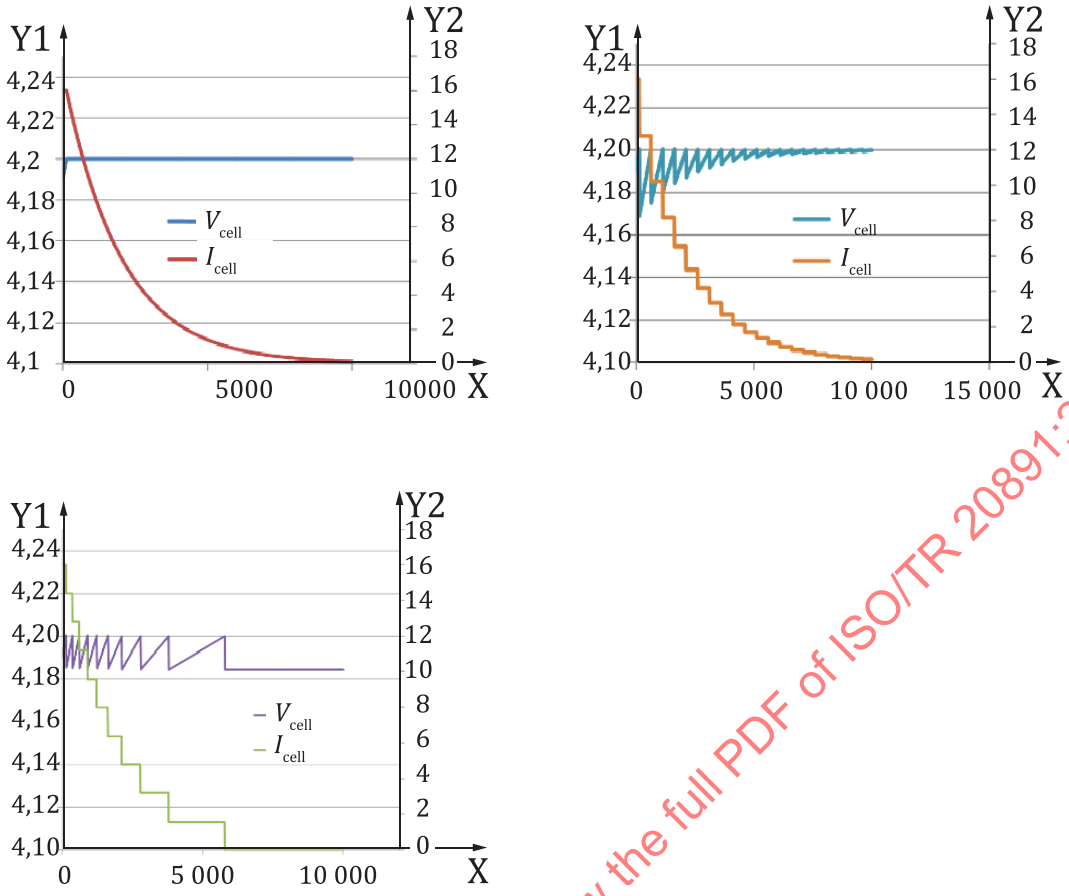

Key

X time (s)

Y1 voltage (V)

Y2 current (A)

Figure 34 — Taper charge management: regulated (left top), by fixed current steps (right top) and by relative current factor (right top)

Obviously the fitting to each type of curve provides a different time constant, even if the battery stays the same, hence the above mentioned uncertainty. As an example, simulating the battery by a simple RC network, the spread in estimated time constant can vary in the range of 1 840 s to 1 973 s when the fixed steps size varies from 1/10 to 1/50 of the initial constant current, the real value being 2 000 s.

6.3.2.3 Round trip efficiency processing

The amount of energy that is lost in the process of restoring the initial SoC after a discharge is obviously correlated to the cell internal resistance, offering an indirect way of assessing its evolution with ageing. This assumes, though, that it is possible to identify two different times at which the SoC is exactly the same. This is exemplified hereafter by the processing of two different sets of test data.

For the first one, the test conditions were these of a LEO orbit at constant DoD. The internal resistance was measured at intervals by a classical delta current method and several consecutive charge/discharge cycles around the same time were processed to derive the round trip efficiency or, in fact, the RTL, defined as:

$$l_{RTL} = \frac{W_{ch} - W_{disch}}{W_{ch}} \tag{10}$$

where

W_{ch} is the energy stored during charge;

W_{disch} is the energy delivered during discharge.

The main results are visible in Figure 35 and Figure 36. It can be seen that the RTL relative change is strongly correlated with the internal resistance one. Several comments are to be made:

— A few samples are missing where data were not available or could not be exploited.

— The match of RTL to internal resistance is not one-to-one. This can be explained by the fact that the direct measurement of the internal resistance provides a value that depends on the test conditions (chiefly on when the voltage is sampled following the current step) while the RTL is affected by all contributors to the internal resistance.

— The test was performed at a constant DoD, therefore the effect of the internal resistance onto the energy loss is not disturbed by fluctuations of the charge or discharge currents.

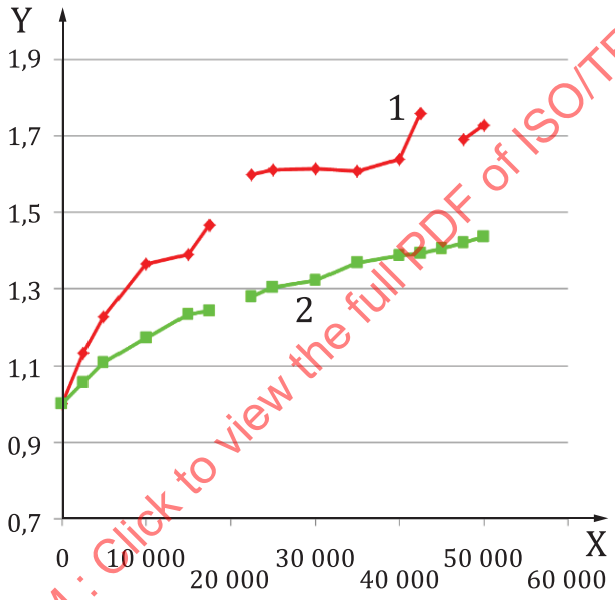

Key

X cycle

Y relative increase from BoL value

1 RTL

2 internal resistance

Figure 35 — Relative increase in RTL (red) and internal resistance versus cycle number

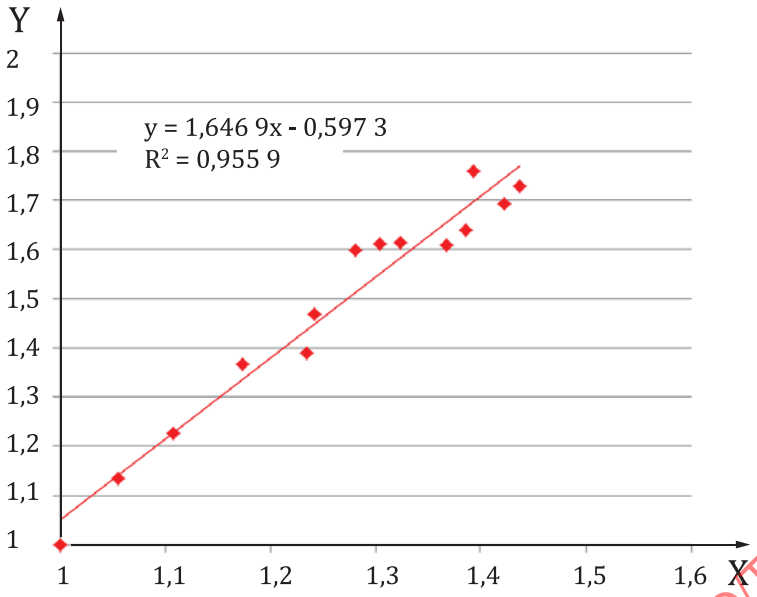

Key

X relative increase in resistance vs. BoL

Y relative increase in RTL vs. BoL

Figure 36 — Relative increase in RTL vs. internal resistance (dots) and linear regression

The second set of data is also a LEO cycling but with the variable load shown in Figure 37:

— The discharge is made under two different levels of constant power drain and has variable durations.

— The charge is done under a fixed and constant current, followed by a tapering phase of variable length, depending on the SoC and remaining time before discharge. The start time of the calculation is taken at the beginning of a discharge and the finish time during a taper (CV) phase when the charge current is the same than it was just before the start time (blue markers in the figure). This ensures that they correspond to the same SoC.

The resulting evolution of RTL and internal resistance are illustrated by Figure 38 and Figure 39.

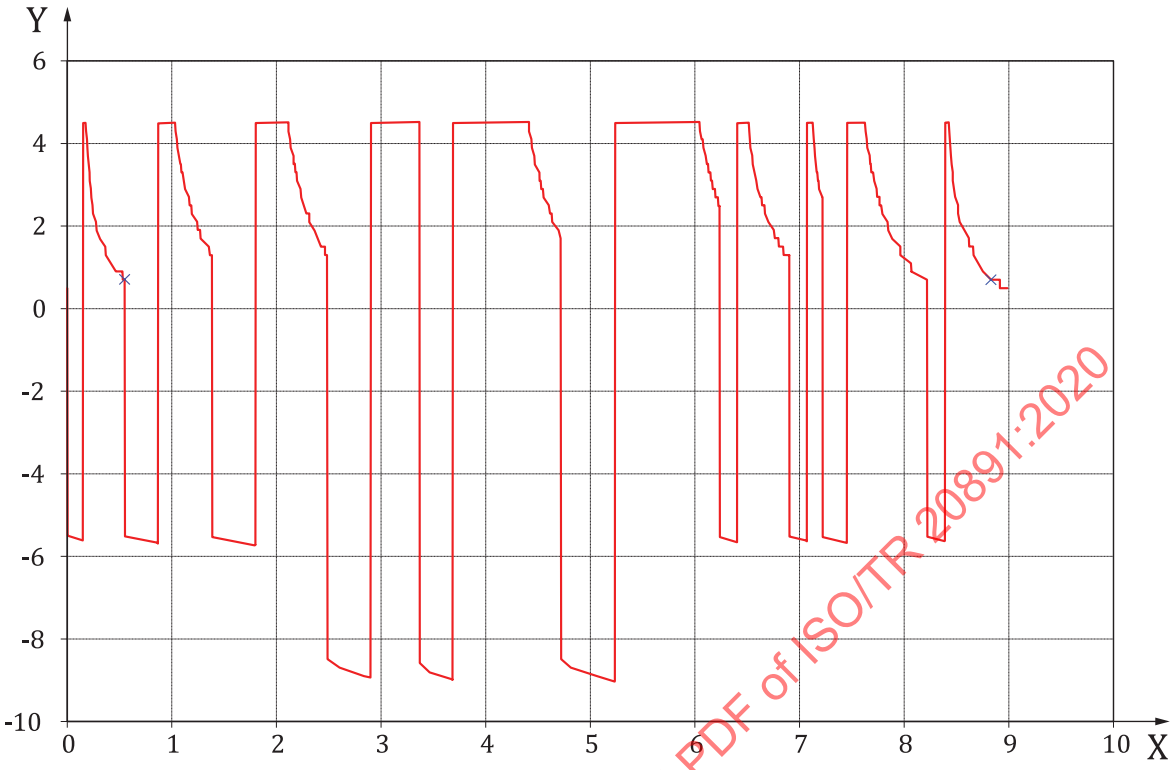

Key

X time (h)

Y $I_{battery}$ (A)

Figure 37 — Current profile of the variable DoD test

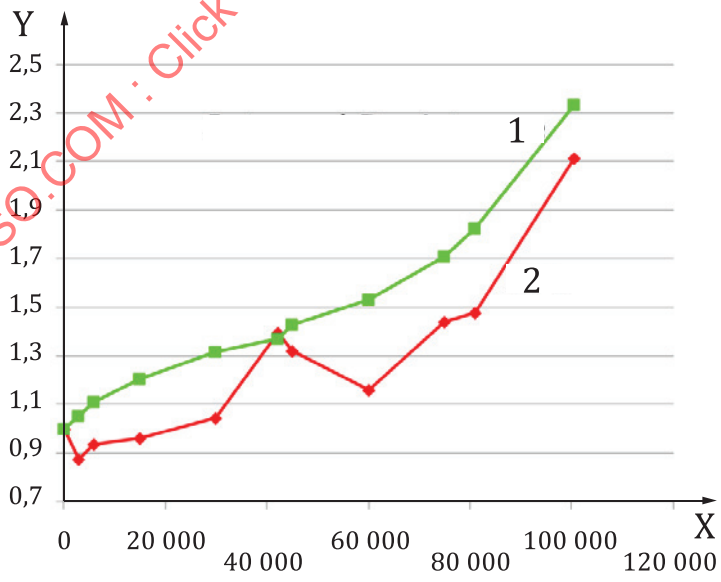

Key

X cycle

Y relative increase in RTL vs. BoL value

1 internal resistance

2 RTL

Figure 38 — Relative increase in RTL (red) and internal resistance versus cycle number